

Quantum Well and Quantum Dot Modeling for Advanced Infrared Detectors and Focal Plane Arrays

David Ting, S. D. Gunapala, S. V. Bandara, C. J. Hill

Jet Propulsion Laboratory, California Institute of Technology



Collaborators

J. K. Liu, E. R. Blazejewski, J. M. Mumolo, S. A. Keo,
Julianne Liu, Joseph Thang
Jet Propulsion Laboratory, California Institute of Technology

S. B. Rafol - *Infravision Systems*

Y.-C. Chang - *U. Illinois at Urbana-Champaign*

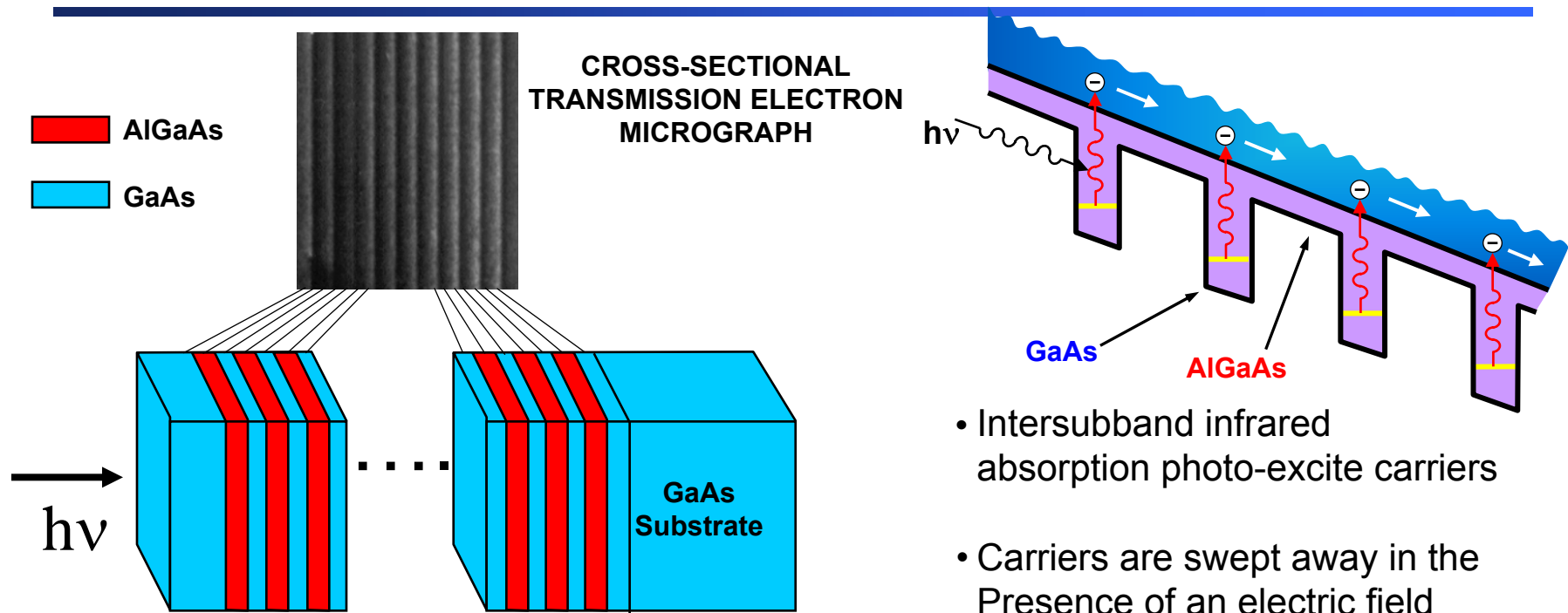
J. Woolaway, C. A. Schott, D. Zalar
FLIR Systems, Indigo Operations

Paul LeVan - *AFRL*

Mark Stegal - *SEIR*

Introduction

QUANTUM WELL INFRARED PHOTODETECTOR (QWIP)
FOCAL PLANE ARRAY TECHNOLOGY

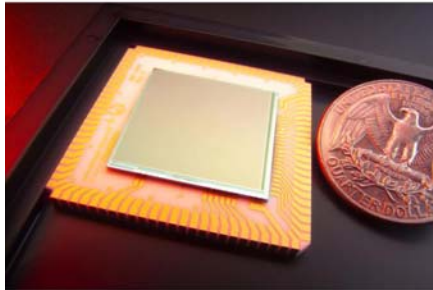


- Designed artificial infrared material based on highly mature GaAs technology.
- Materials flexibility allows for highly customizable design
 - QWIPs in 4 – 20 μm wavelength range produced routinely.
 - Narrow-band, broad-band, spatially-separated multiband, pixel co-located simultaneous dual-band.
 - Thermal imaging, hyperspectral and multispectral spectrometry, target identification.

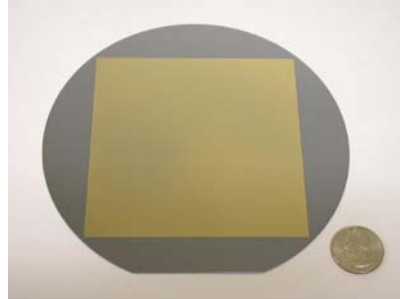
Advantages of QWIP Focal Plane Arrays

- Large format, affordable FPA with high fill factor, high uniformity, negligible 1/f noise, and high radiation hardness

Size Comparison of Two Available QWIP Detector Arrays

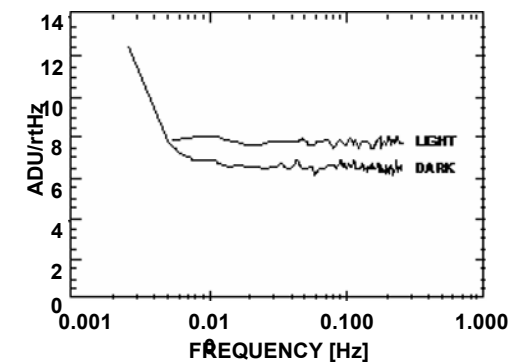


JPL 1024 x 1024 Pixel QWIP Focal Plane Array



4096 x 4096 Pixel QWIP Detector Array on 6-inch GaAs Wafer

QWIP Stability



1/f Noise of QWIP Focal Plane Array

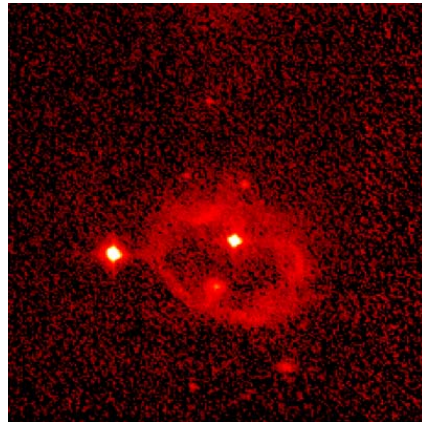
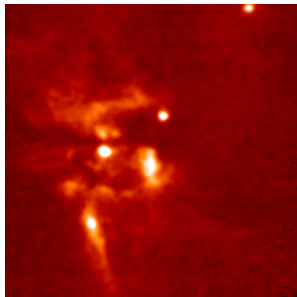
- **Mature III-V Material Growth & Processing Technology**
 - High Uniformity
 - High Operability
 - High Reliability
 - Mature Manufacturability
- **High Yield**
 - Low Cost
- **Tailorable Wavelength**
 - 3 to 16 μm , multi-band and broadband
- **Portable IR QWIP Camera Available**
- **Low Power Dissipation**
 - Large RoA
- **Low 1/f Noise**
 - No 1/f Noise Down to 10 mHz
- **No Delamination Due to Temperature Recycling**
 - Extremely Stable QWIP-ROIC Interface
 - No Pixel Outages/Array Delaminations After Thousands of Cycles
- **Radiation Hard**

Temporal Stability Facilitates Systems Design



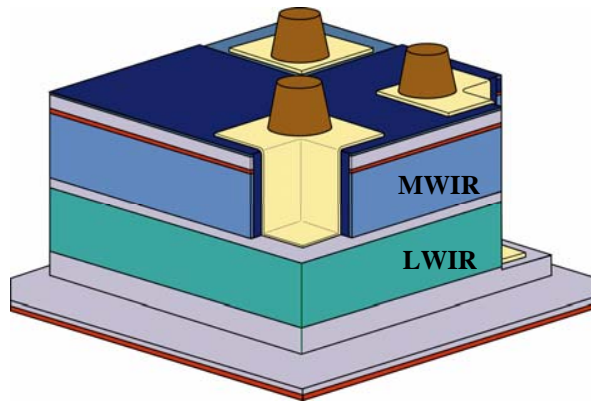
Palm-size with 256x256 FPA (1998)

- Low 1/f noise.
 - No 1/f noise down to 30 mHz.
- Excellent temporal stability
 - Non-uniformity correction table stored in EPROM.
 - Unchanged since 1998.
- Multi-hour exposure without constant re-calibration. Capable of long-integration time applications.

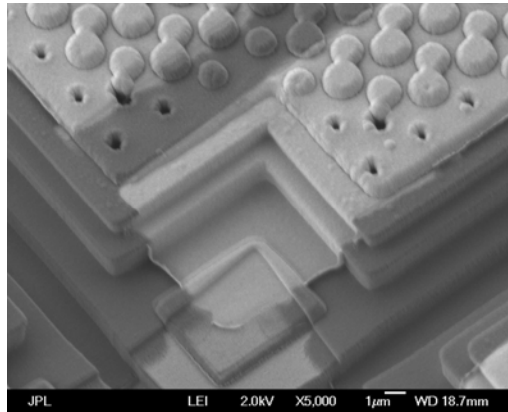


8.5 μm mid-infrared image, obtained with a QWIP focal plane array at primary focus of the Palomar 200-inch Hale telescope.

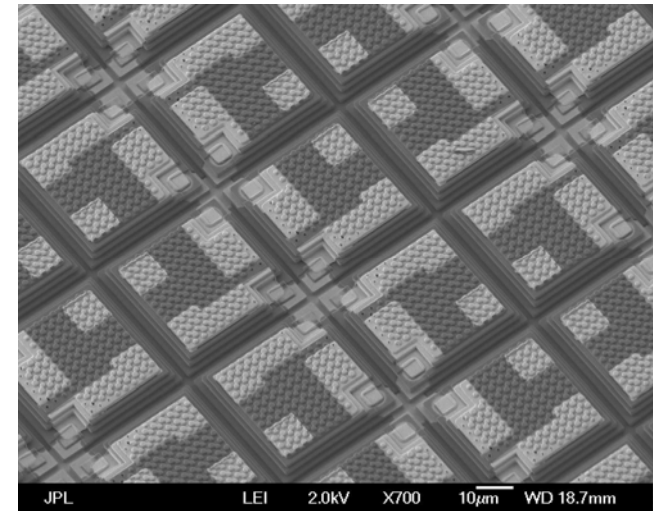
True Pixel Co-registered, Simultaneously Readable Dualband QWIP FPA



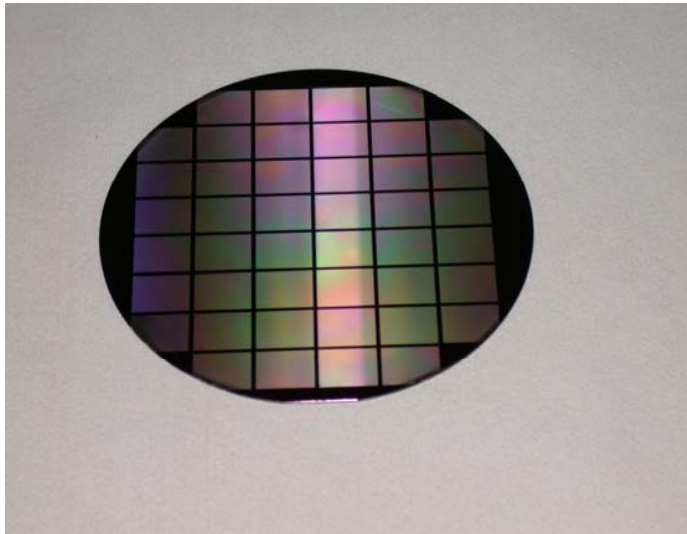
Dualband pixel architecture



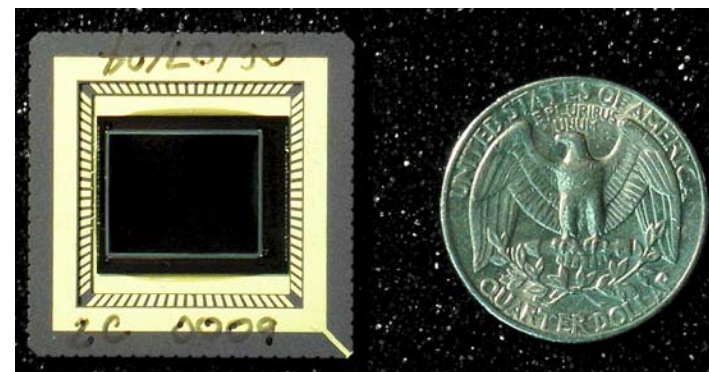
SEM of metal via connects



SEM of dualband QWIP array



4-inch GaAs wafer with
48 detector dies



320x256 pixels Dualband
QWIP FPA HYBRID

Dualband QWIP FPA Pathfinder



LWIR

MWIR

Features to look for,

The cigarette lighter produce lots of hot CO₂ gas. So, flare is broader MWIR due to CO₂ emission, where as LWIR (8-9 microns) doesn't have any emission (just the heat).

The hot cigarette lighter flame produce so much MWIR signal, it reflects off from the lens and Jason's face.

The plastic piece Jason is holding is opaque in LWIR, but transparent in MWIR.

Format	- 320x256 pixels, dualband & pixel co-registered
Wavebands	- 4.4-5.1 & 8-9 μm
NE Δ T	- 22 & 24 mK for 300K background with f/2 optics
QE	- 19% & 15%
Photoconductive gain	- 0.5 & 0.3
Detectivity	- $> 2 \times 10^{11}$ & 1×10^{11} Jones
Operating temp.	- 65 K
Fill factor	- $> 85\%$

Current QWIP Development: Implication for QDIP

- JPL is currently in the process of developing 1K x 1K, simultaneous MWIR-LWIR true dual band QWIP FPA
 - Realistic plans for extension to 2K x 2K already in place
 - Leading edge in infrared FPA technology
- The same large-format dual-band FPA technology can be applied to Quantum Dot Infrared Photodetector (QDIP) with **no modification**, once QDIP exceeds QWIP in single device performance !

From QWIP to QDIP

- The QDIP shares all the positive attributes of QWIP
 - Based on the same mature material systems and processing technology
- The QDIP also has the following advantages over QWIPs
 - Capable of normal incidence absorption, can lead to higher quantum efficiency
 - Capable of higher operating temperature
- QDIP has the potential to out-perform the QWIP, while retaining all of the QWIP advantages.

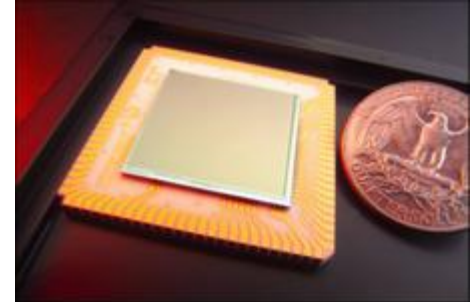
Why Quantum Dot Infrared Photodetectors ?

- High spatial uniformity
 - Reduces need for complex non-uniformity correction circuitry
 - Facilitates large-format FPA fabrication
- Excellent temporal stability
 - Eliminates need for frequent recalibration, simplifies system design
- High quantum efficiency and D^*
 - Capable of reaching theoretical ideal photoconductor background limited D^* (BLIP limit) for 300K background with f/2 optics
- Increased operating temperature
 - Can achieve the same NE Δ T at higher operating temperatures
 - Less demand on cooler, longer system lifetime
- Based on mature wide-band gap III-V semiconductors
 - Excellent manufacturability
 - Faster turn-around, higher availability, lower cost

Quantum Dot Based LWIR FPAs

✓ Build on JPL's proven track record of delivering infrared FPAs based on quantum effects in III-V photodetectors

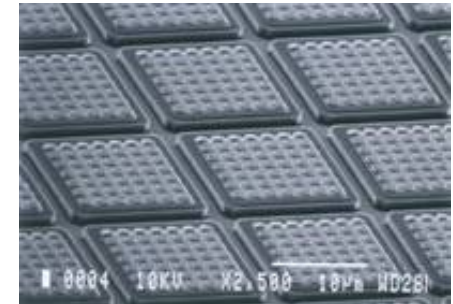
- Large format
- Excellent uniformity
- Excellent operability
- Low $1/f$ noise
- Thinned arrays eliminate
 - Optical crosstalk
 - Thermal mismatch with ROIC
 - Pixel delamination



1024x1024 MWIR FPA
Designed, grown, and fabricated at JPL

+ Add quantum dots to this current capability

- Normal incidence absorption
- Higher temperature operation (lower dark current)
- Higher responsivity (longer lifetime)
- Further increase the radiation hardness



Individual pixels in an FPA, with integrated grating structure

= **New generation of high performance high operating temperature infrared focal plane arrays**

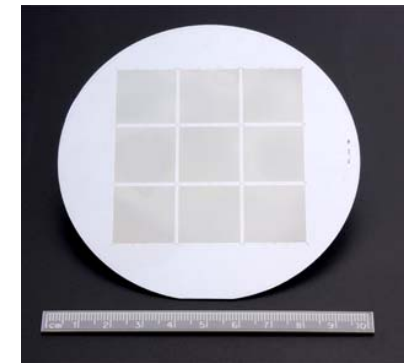
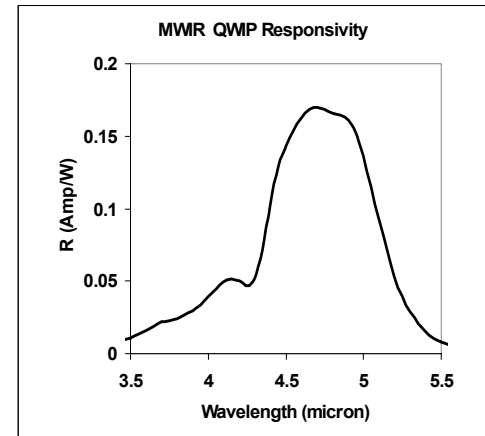
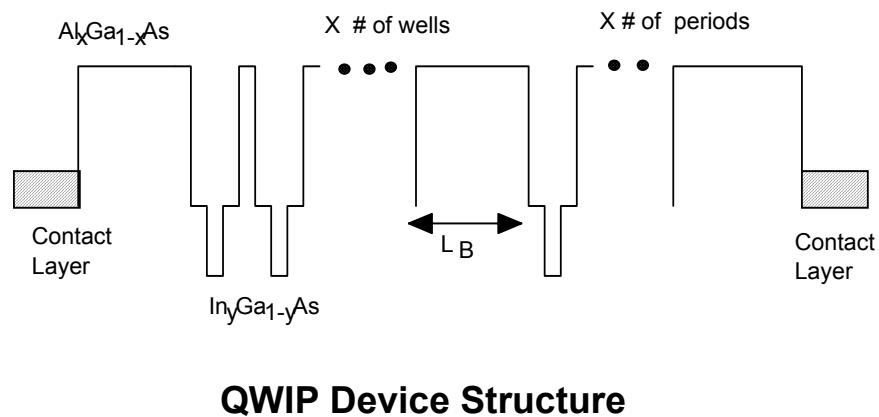
Development of Megapixel MWIR & LWIR QWIP Focal
Planes Arrays & 320 x 256 Pixel Dualband QWIP Focal
Plane Arrays

OUTLINE

- **1K x 1K MWIR Focal Plane Array**
- **1K x 1K LWIR Focal Plane Array**
- **320 x 256 Dual-band FPA & Camera**
- **Summary**

1024 x 1024 PIXEL MWIR CAMERA

BROADENED MWIR RESPONSE FOR SPECIFIC DOD APPLICATION



Nine 1024 x 1024 QWIP Focal Plane Arrays (FPAs) on 4-inch GaAs Wafer

- Increased the spectral coverage by utilizing a multi-coupled-quantum-well structure for tracking missiles during boost phase.
- Grown on 4-in GaAs wafers.

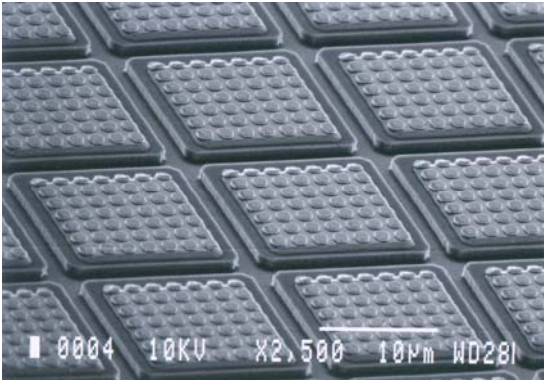
- S. V. Bandara, S. D. Gunapala, J. K. Liu, E. M. Luong, J. M. Mumolo, W. Hong, D. K. Sengupta, and M. J. McKelvey, "10-16 μm Broadband Quantum Well Infrared Photodetector", *Appl. Phys. Lett.* **72**, 2427 (1998).
- * Sarath D. Gunapala, Sumith V. Bandara, John K. Liu, Sir B. Rafol, and Jason M. Mumolo, "640x512 Pixel Long-wavelength Infrared Narrowband, Multiband, and Broadband QWIP Focal Plane Arrays" *IEEE Trans. Electron Devices*, **50**, pp. 2353-2360, 2003.

1024X1024 PIXEL QWIP FPA SPECIFICATIONS FOR THIS APPLICATION

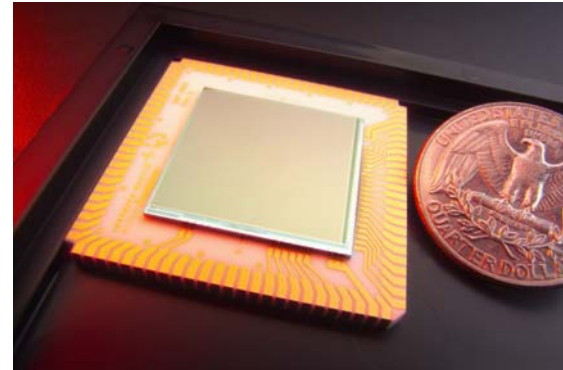
SPECTRAL RANGE	- 4.4 - 5.1 μm
PIXEL PITCH	- 19.5 μm
PIXEL ACTIVE AREA	- 17.5 x 17.5 μm^2
ABSORPTION (peak) Q.E.	- 19%
GAIN	- 0.3
RESPONSIVITY	- 0.27 A/W
OPERATING TEMP.	- 80 - 110 K
FRAME RATE	- 30 Hz
NON-U (UNCORRECTED)	- 5.6%
NON-U (CORRECTED)	- 0.05%
OPERABILITY	- 99.98%
NEF*	- 2×10^{-16} W/cm ²
OPTICS	- f/2.3; 400 mm & f/2; 38 mm



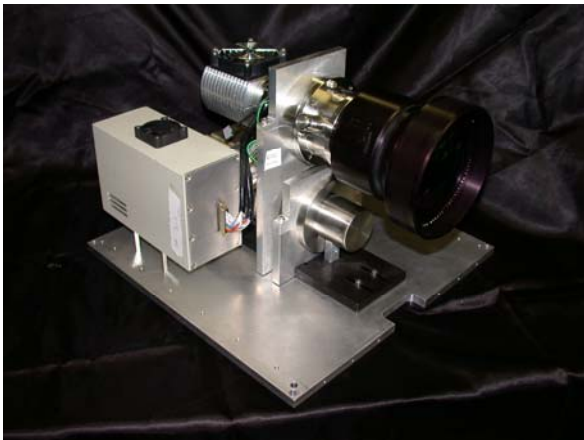
1024X1024 PIXEL MWIR QWIP FPA AND CAMERA DELIVERED TO THIS APPLICATION



Detector pixel with light coupling gratings



1024 x 1024 pixel QWIP focal plane array



1Kx1K MWIR sensor engine



1Kx1K MWIR QWIP camera

1024 x 1024 PIXEL QWIP FPA IMAGERY



➤ NE Δ T OF 19 mK WAS ACHIEVED.

DETECTIVITY AND NEF

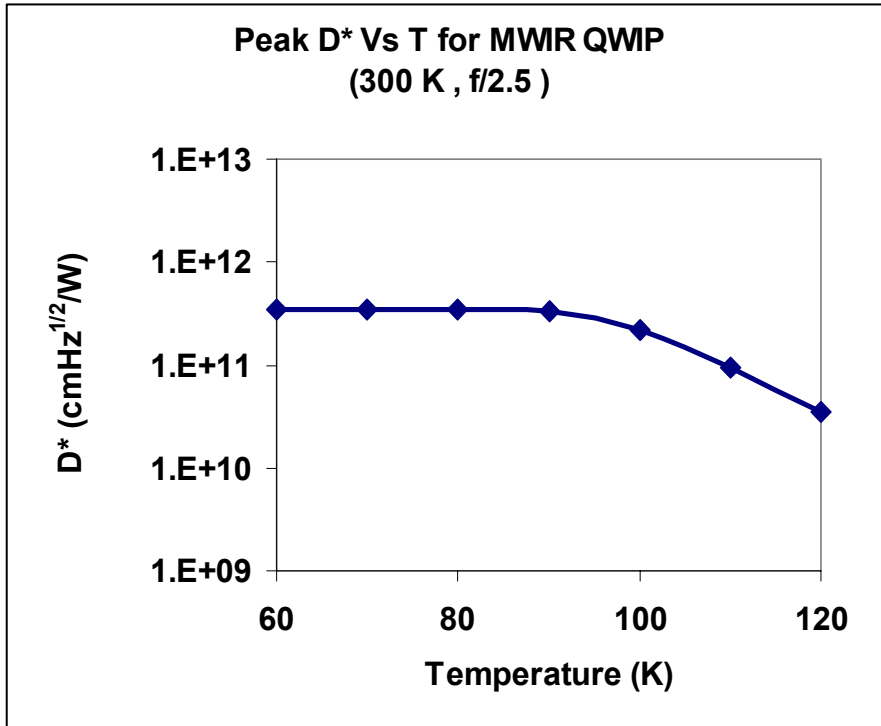
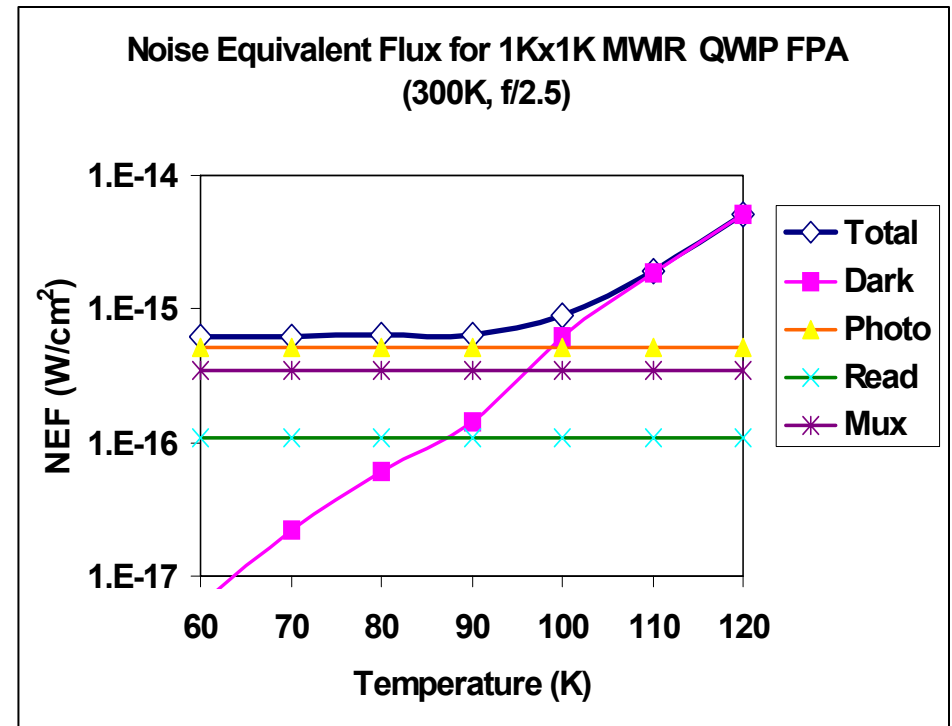
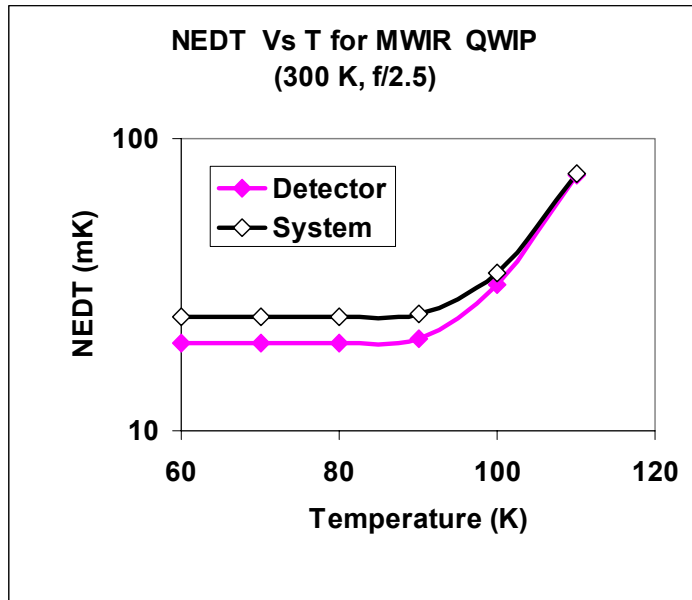


IMAGE OF THE EXIT SLIT
OF MONOCHROMATOR

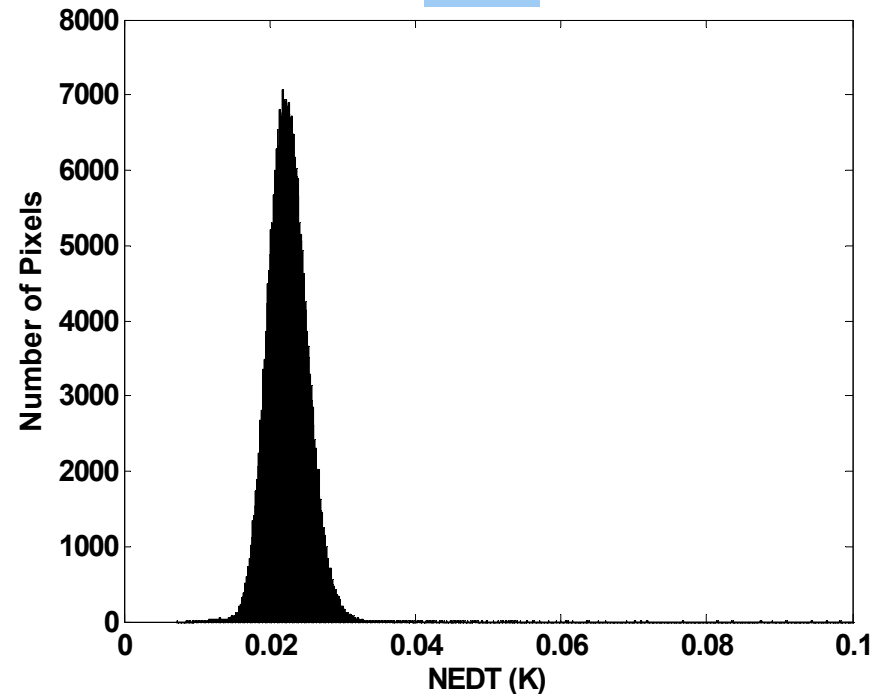


NORMALIZED SPECTRAL RESPONSE

NE Δ T



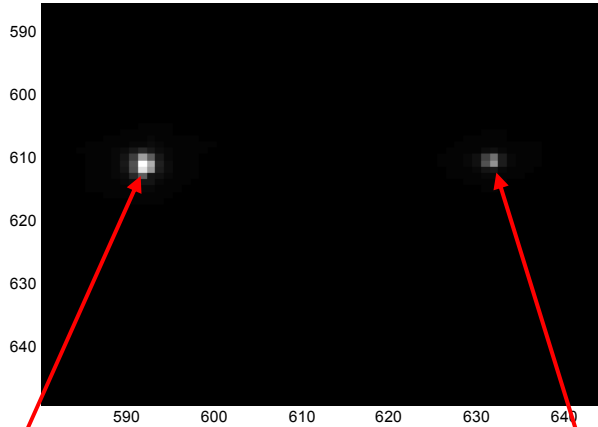
**NOISE EQUIVALENT TEMPERATURE
DIFFERENCE**



- NE Δ T = 22 mK (= 19 mK if ADC noise is subtracted)
- Uniformity = 0.03%
- Operability = 99.5%

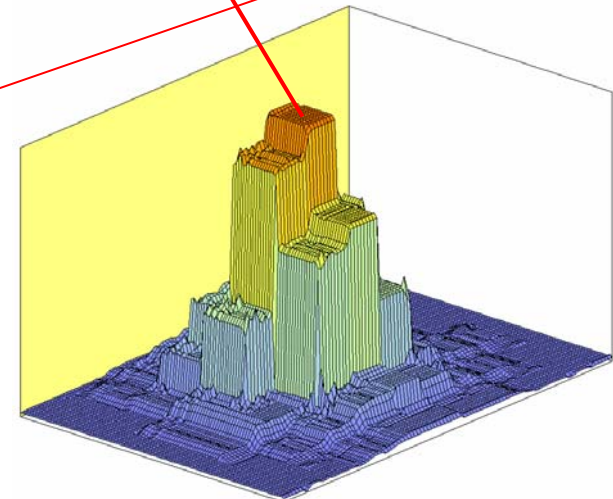
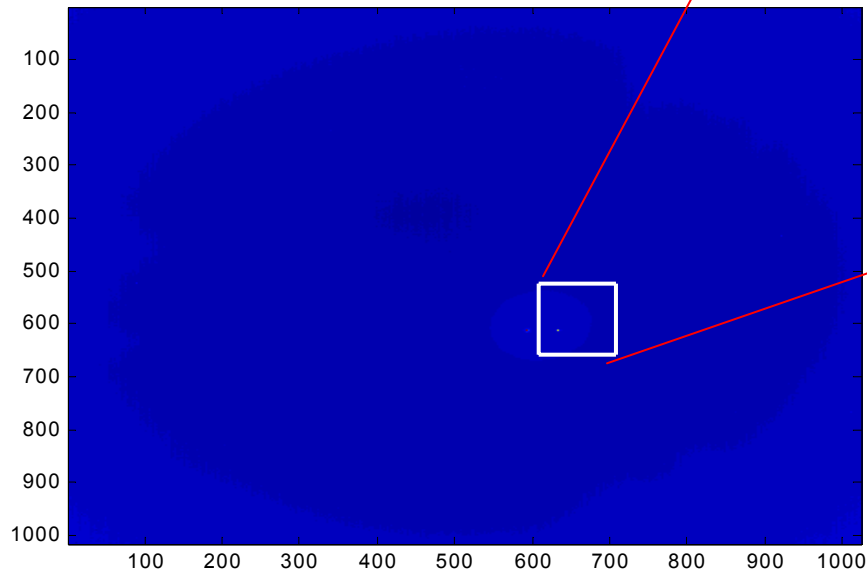
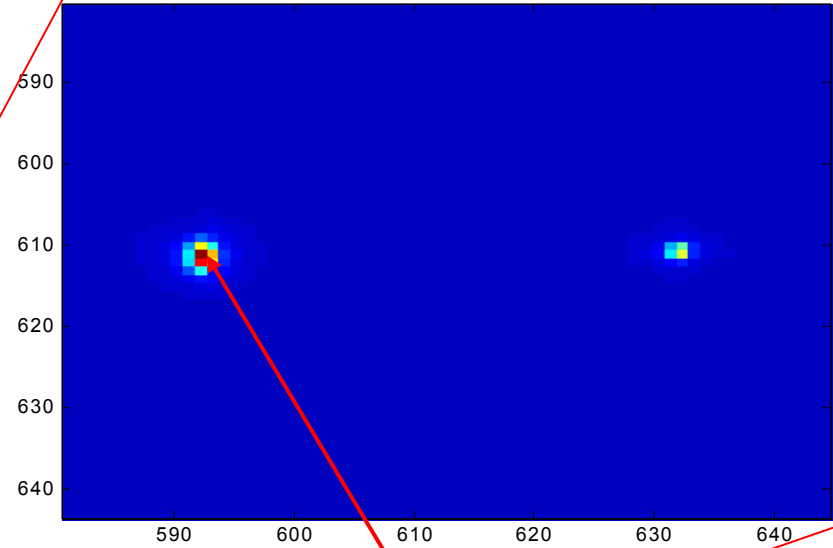
POINT SPREAD FUNCTION

DIFFERENCE IMAGE

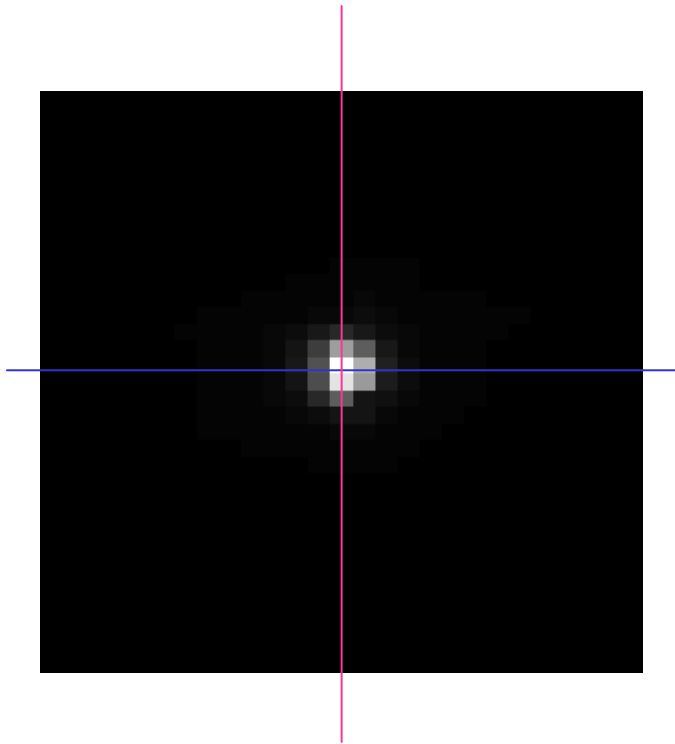


Primary Image

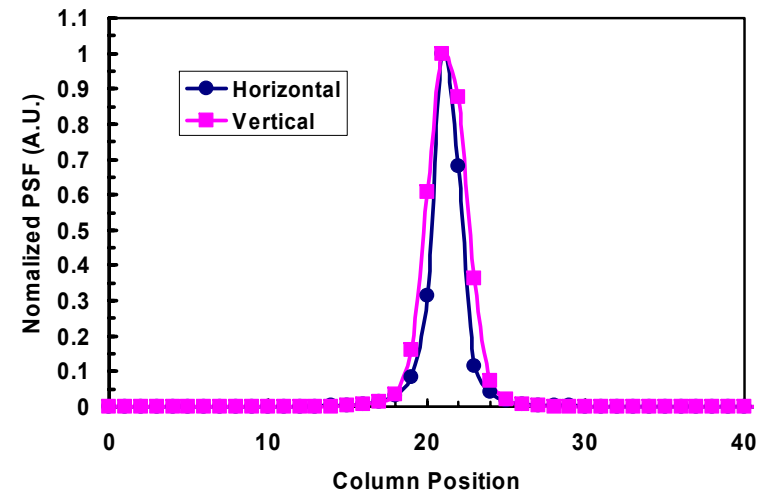
Reflected Image



CROSS SECTION OF 3-D PSF



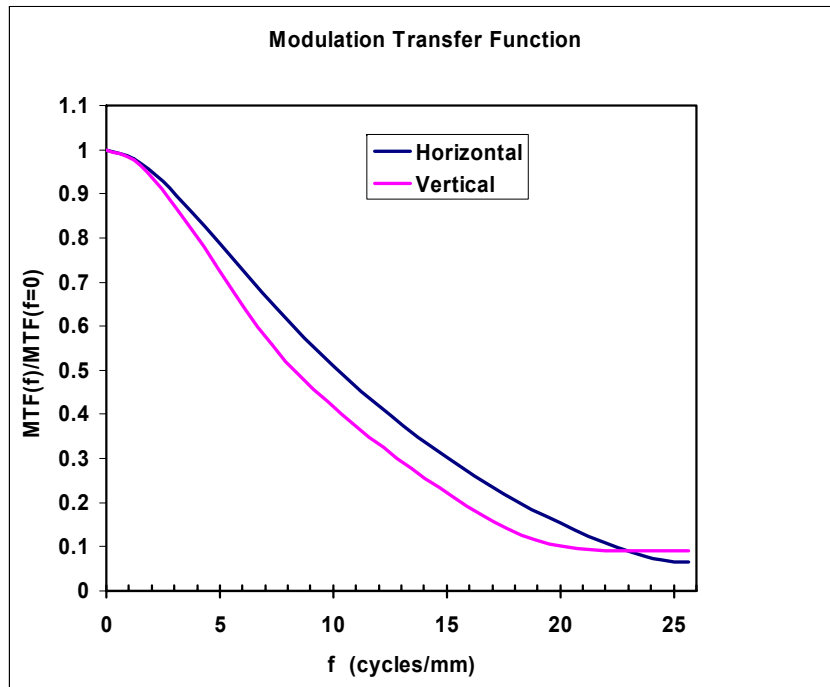
POINT SPREAD FUNCTION



POINT SPREAD FUNCTION

MODULATION TRANSFER FUNCTION

MTF WITHOUT LENS CORRECTION

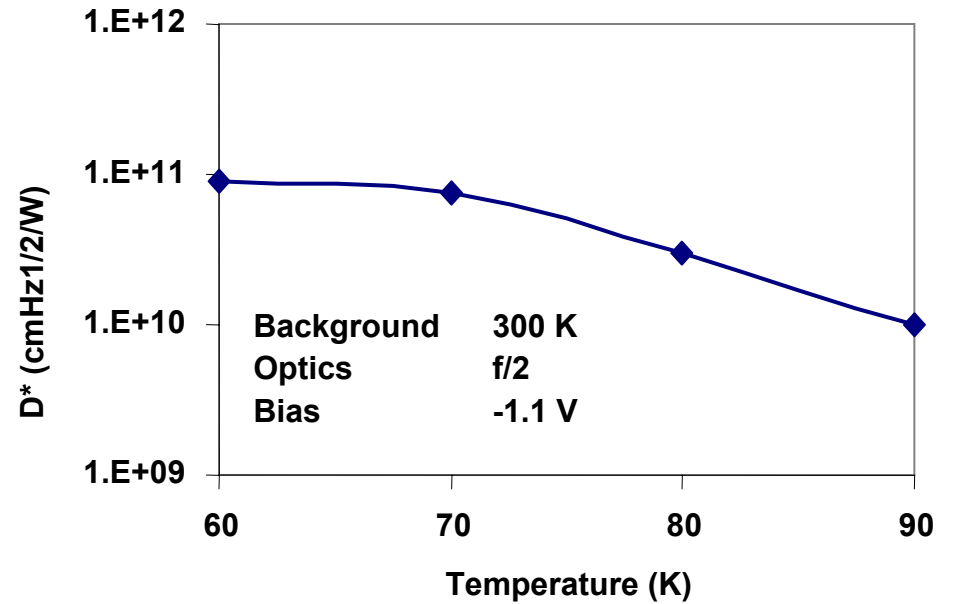
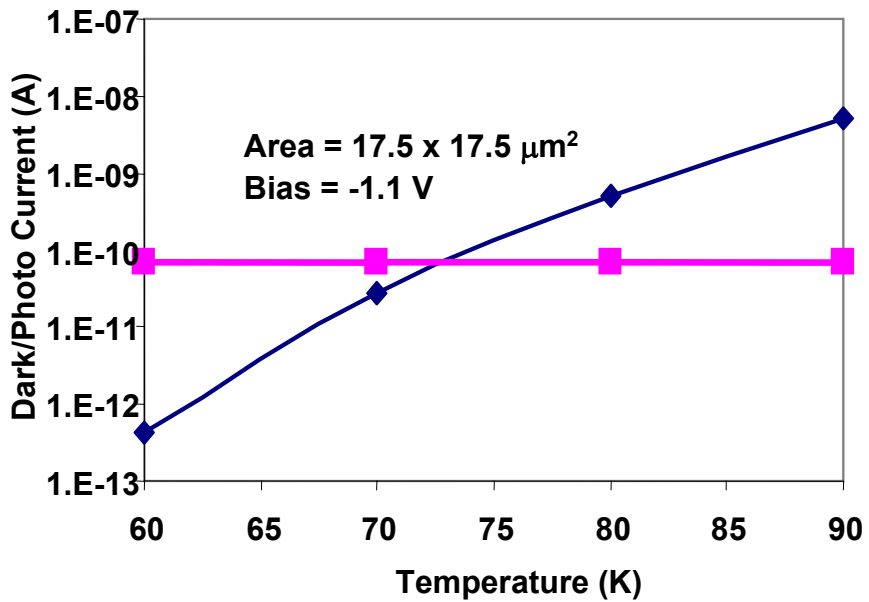
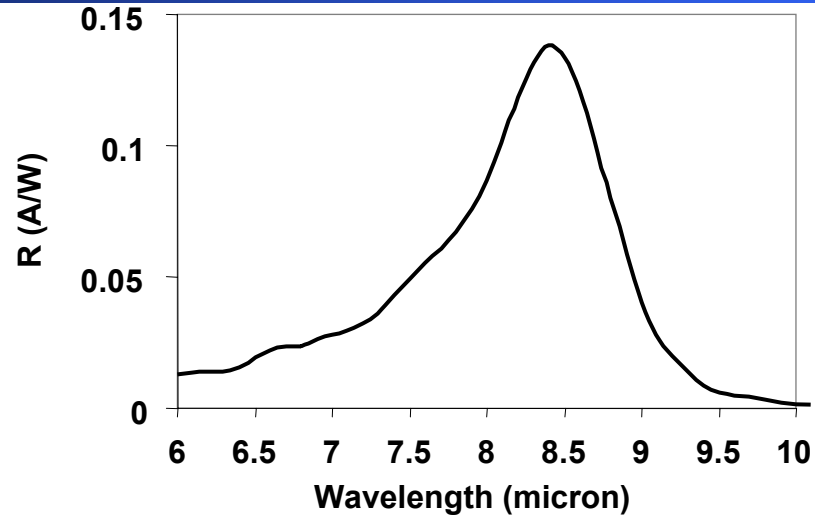


MTF of Lens	– 0.2
Pixel Pitch	– 19.5 μm
Nyquist Frequency	– 25.6 Cy/mm

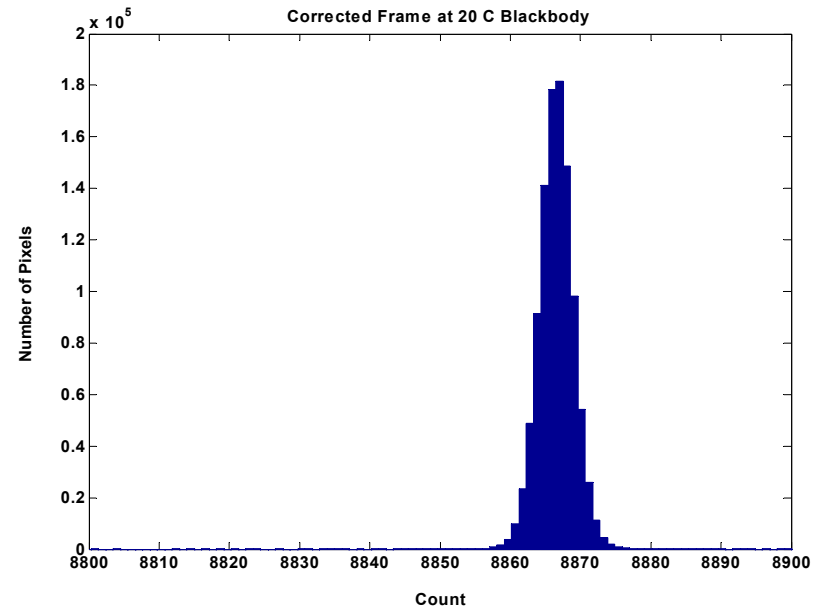
$$\begin{aligned} \text{MTF}_{\text{system}} &= \text{MTF}_{\text{framegrabber}} \times \text{MTF}_{\text{cabling}} \times \text{MTF}_{\text{focalplane}} \times \text{MTF}_{\text{lens}} \\ \text{MTF}_{\text{framegrabber}} \times \text{MTF}_{\text{cabling}} \times \text{MTF}_{\text{focalplane}} &= 0.5 \\ \text{MTF}_{\text{focalplane}} &> 0.5 \end{aligned}$$

1024 x 1024 PIXEL LWIR CAMERA

FIGURES OF MERIT



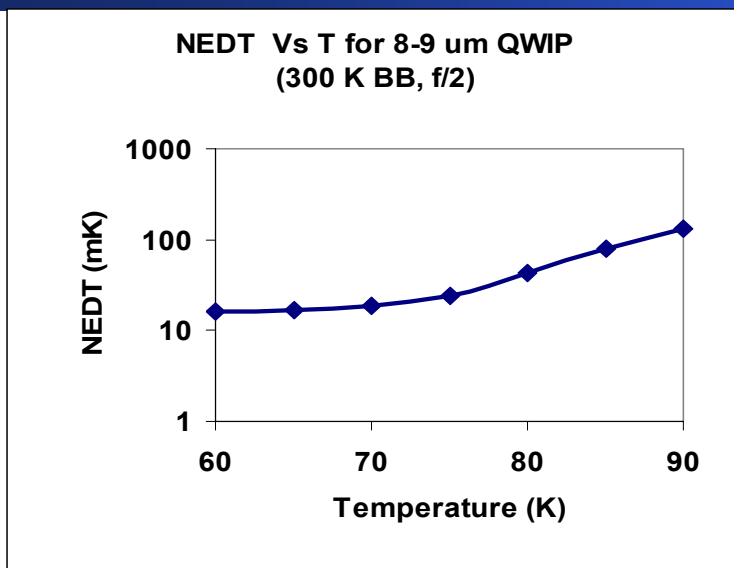
CORRECTED IMAGE



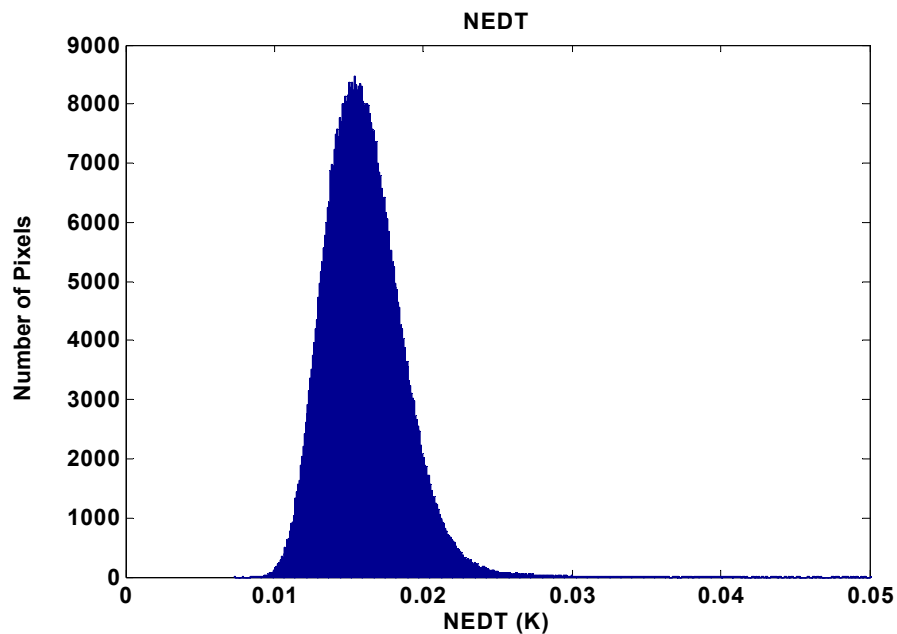
Nonuniformity ~ 0.8 %

Operability ~ 99.98%

NE Δ T



NE Δ T = 16
Window Transmission Assume 95 %
Detector Bias = 1 V,
Integration time = 29 msec,
Operating Temperature = 67 K



$$n_{\text{sys}}^2 = n_{\text{Detector}}^2 + n_{\text{ADC}}^2 + n_{\text{MUX}}^2$$

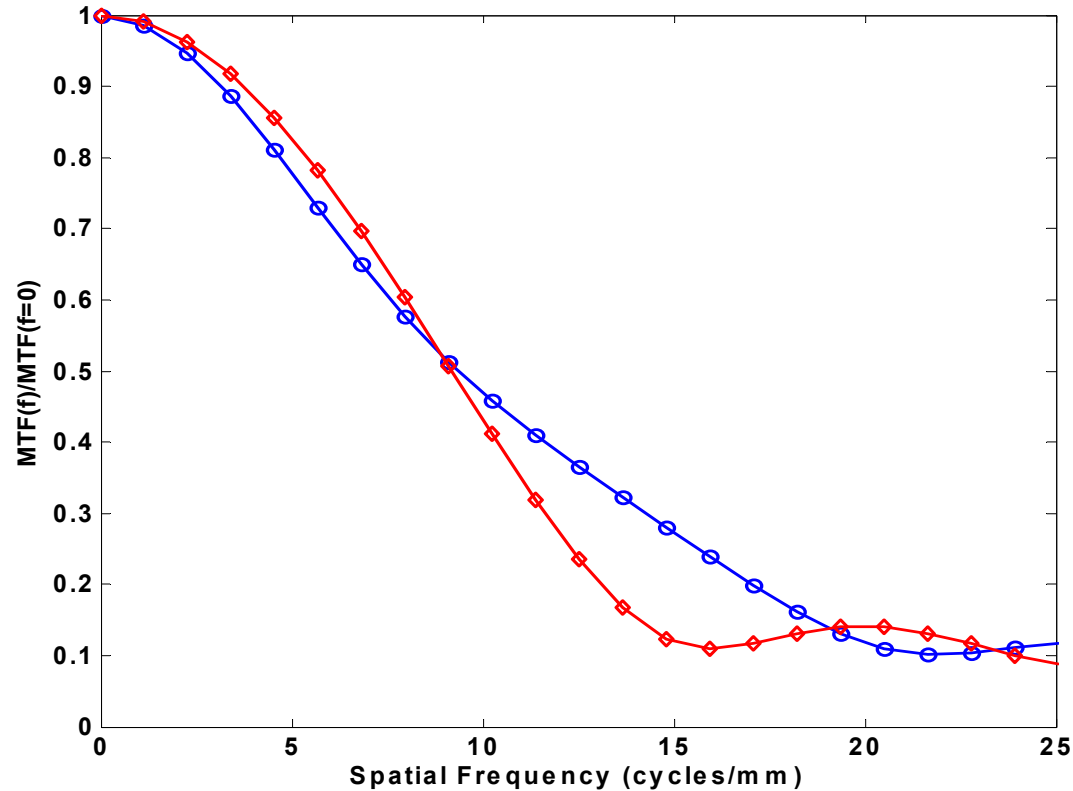
$$2.4^2 = n_{\text{Detector}}^2 + 0.8^2 + 1.0^2$$

$$n_{\text{Detector}} = 2.0$$

$$\text{NEDT}_{\text{Detector}} = 13 \text{ mK}$$

MODULATION TRANSFER FUNCTION

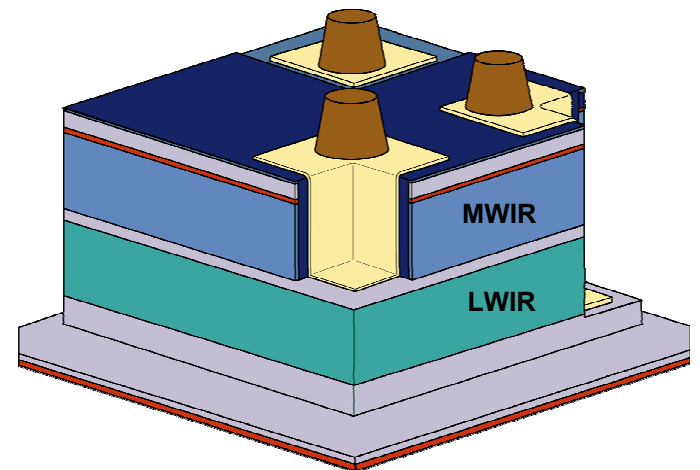
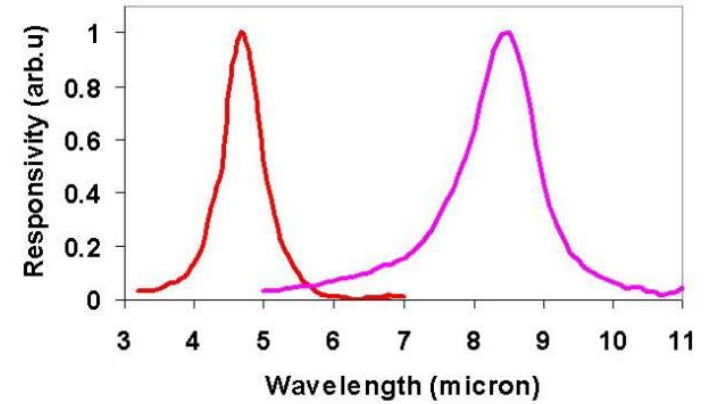
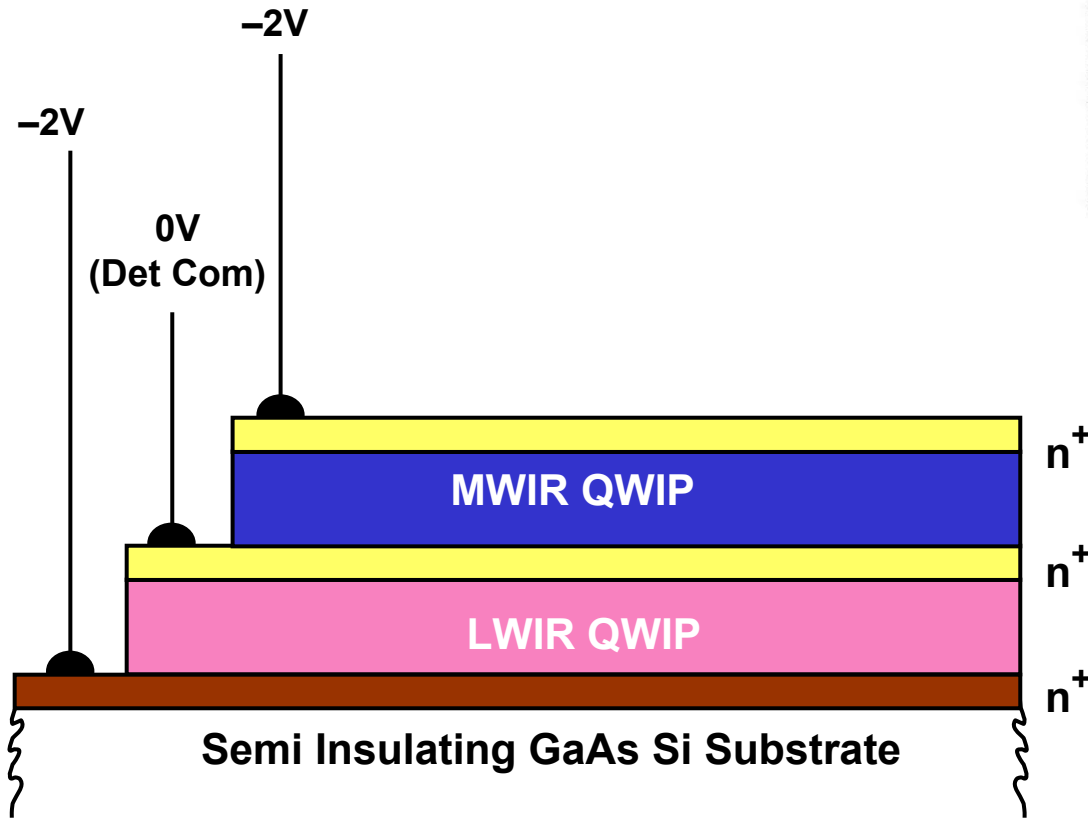
MTF Without Lens Correction



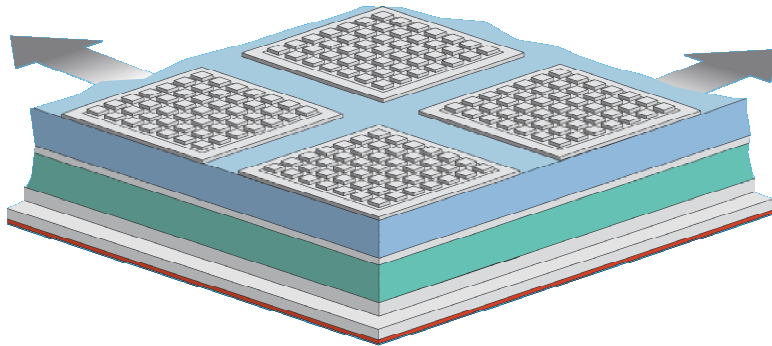
- **Blue Horizontal MTF**
- **Red Vertical MTF**
- **Diffraction Limit at ~ 21 cyc/mm, $f/\# = 2.3$**
- **Nyquist at ~ 25.6 cyc/mm**
- **$MTF_{\text{focalplane}} > 0.5$**
- **Frequency above 21 cyc/mm is not justified since it is beyond diffraction limit blurred circle.**

**PIXEL CO-REGISTERED
SIMULTANEOUSLY READING
DUALBAND (MWIR & LWIR) QWIP
FPA**

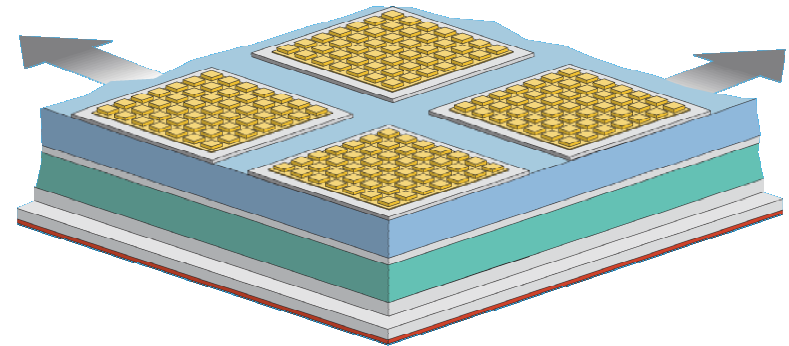
DUAL-BAND (MWIR & LWIR) DETECTOR



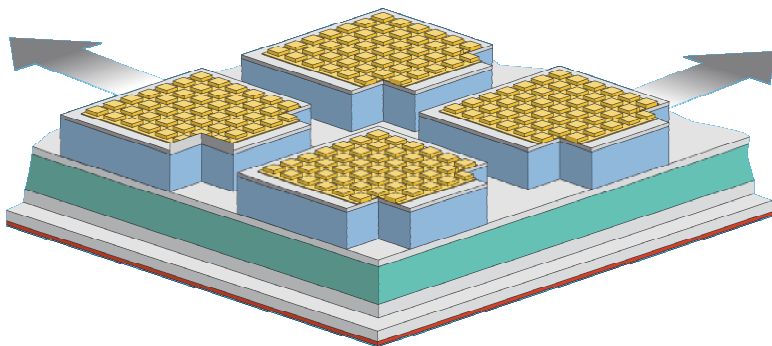
DUAL-BAND FPA FABRICATION PROCESS



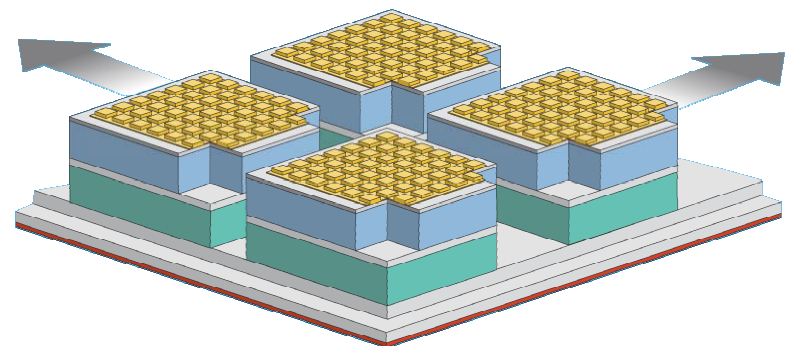
Grating Etch



Top Metal Deposit

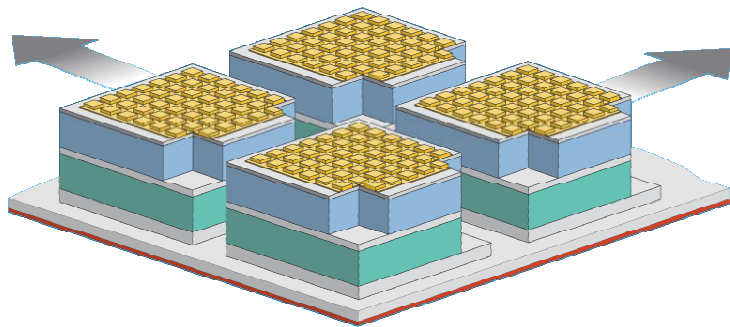


First Mesa Etch

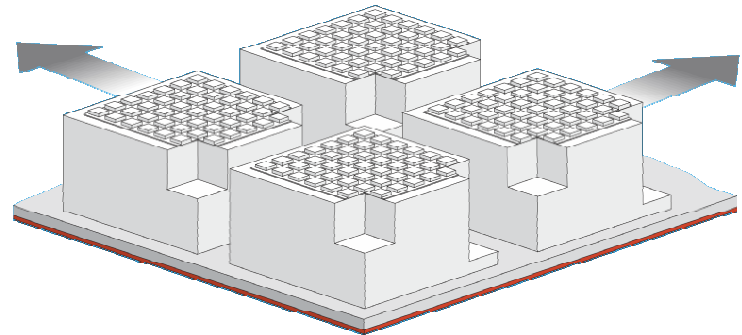


Second Mesa Etch

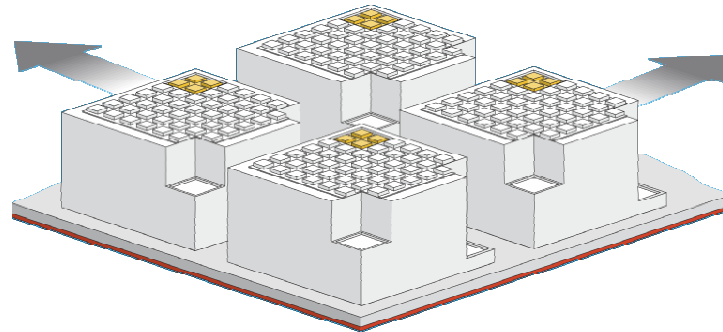
DUAL-BAND FPA FABRICATION PROCESS



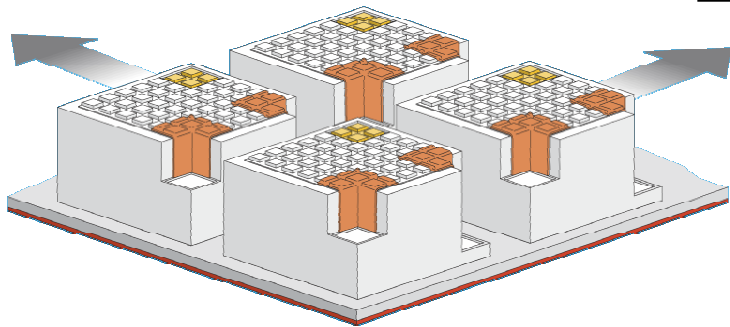
Isolation Etch



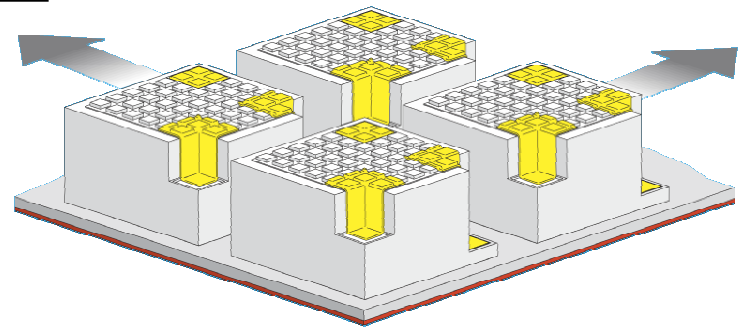
Deposit Insulation Layer



Window Opening

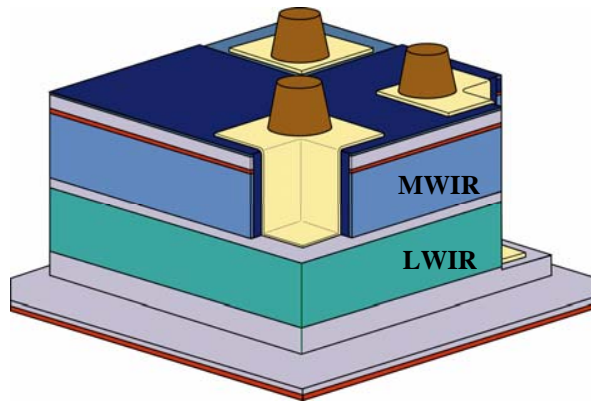


Adhesion Metal Deposit

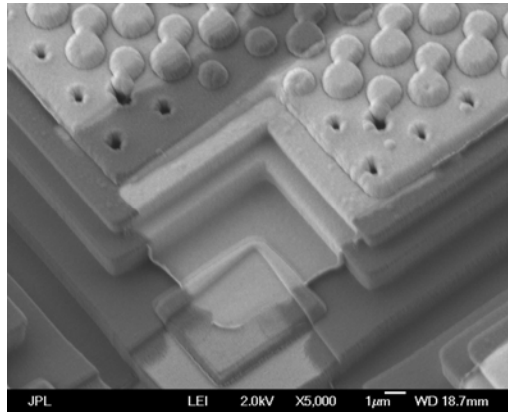


Final Metal Deposit

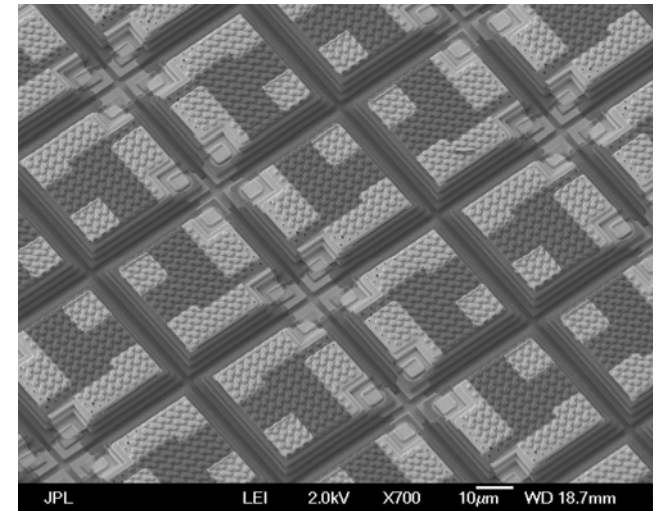
PIXEL CO-LOCATED SIMULTANEOUSLY READABLE DUALBAND QWIP FPA



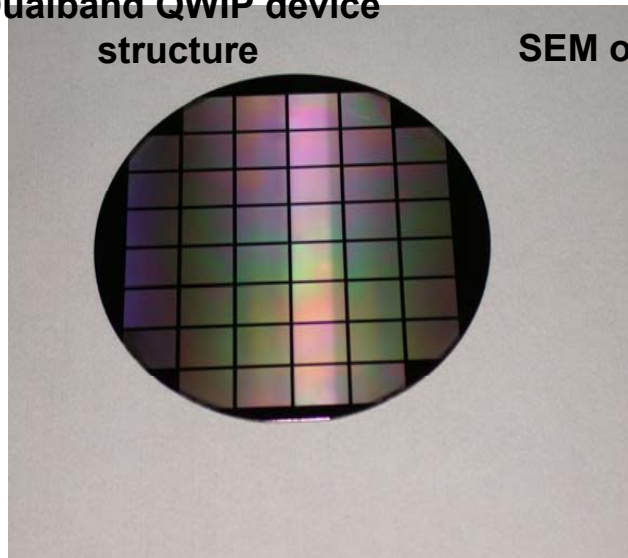
Dualband QWIP device structure



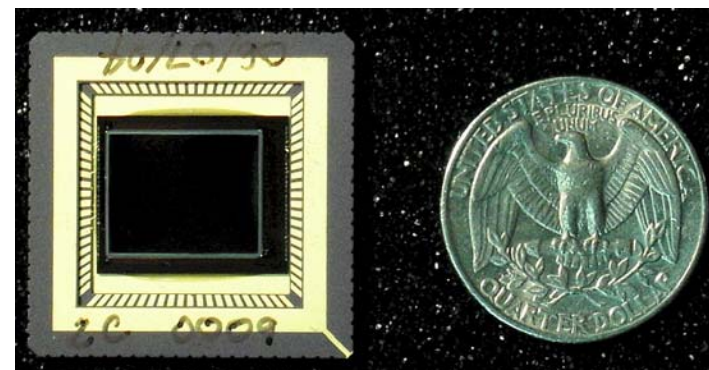
SEM of metal via connects



SEM of dualband QWIP array

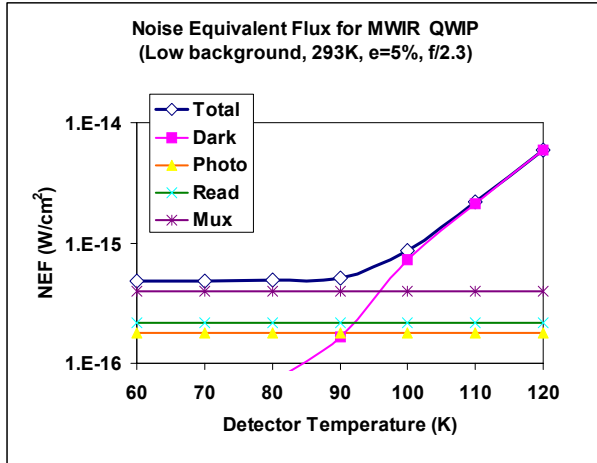


4-inch wafer with 48 detector dies

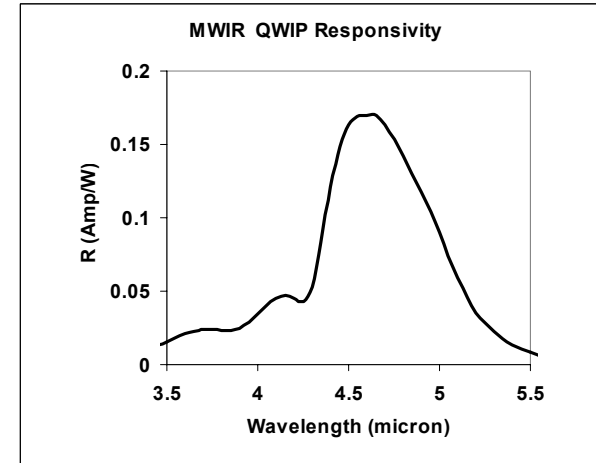


Dualband QWIP FPA
HYBRID

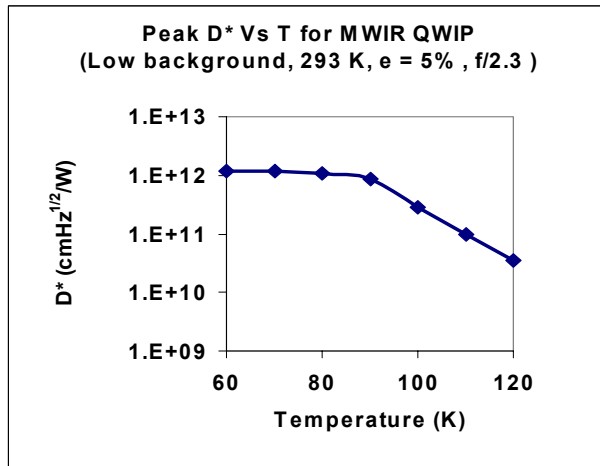
DUALBAND QWIP – MWIR LOW BACKGROUND



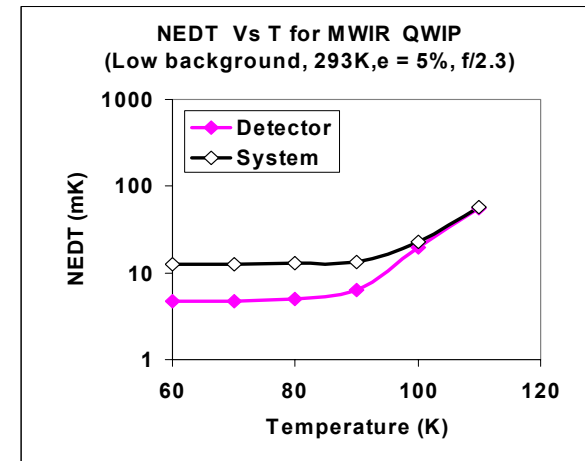
NEF



RESPONSIVITY

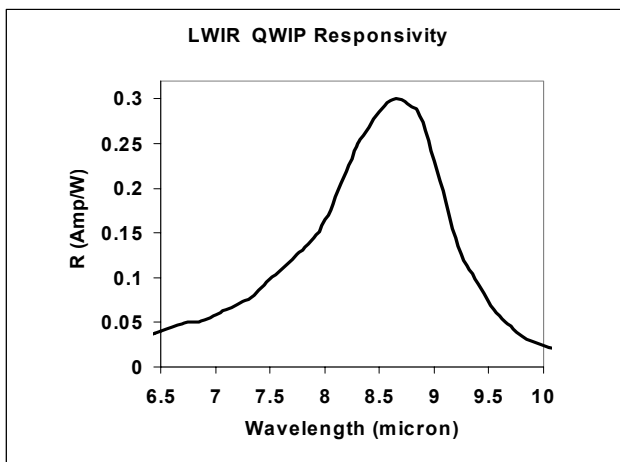


DETECTIVITY

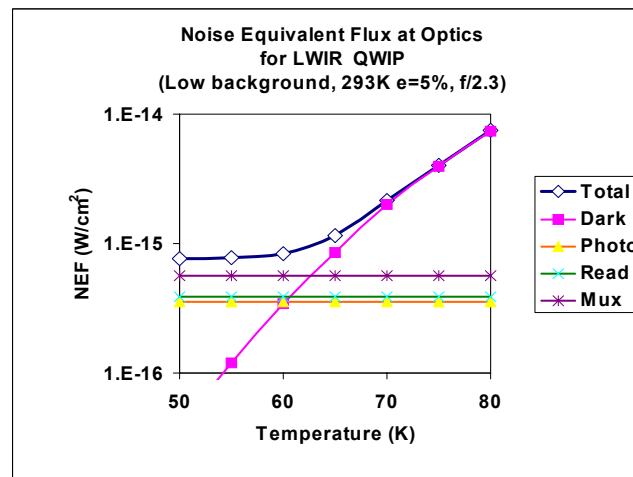


NEDT

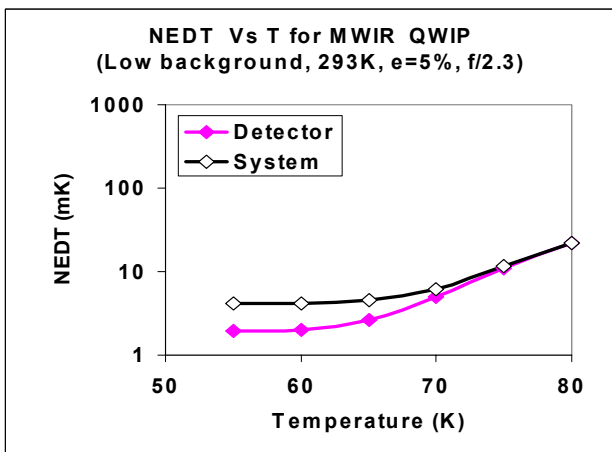
DUALBAND QWIP – LWIR LOW BACKGROUND



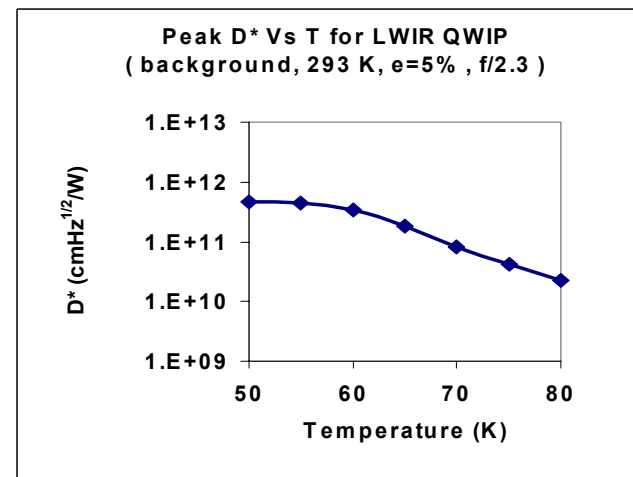
RESPONSIVITY



NEF

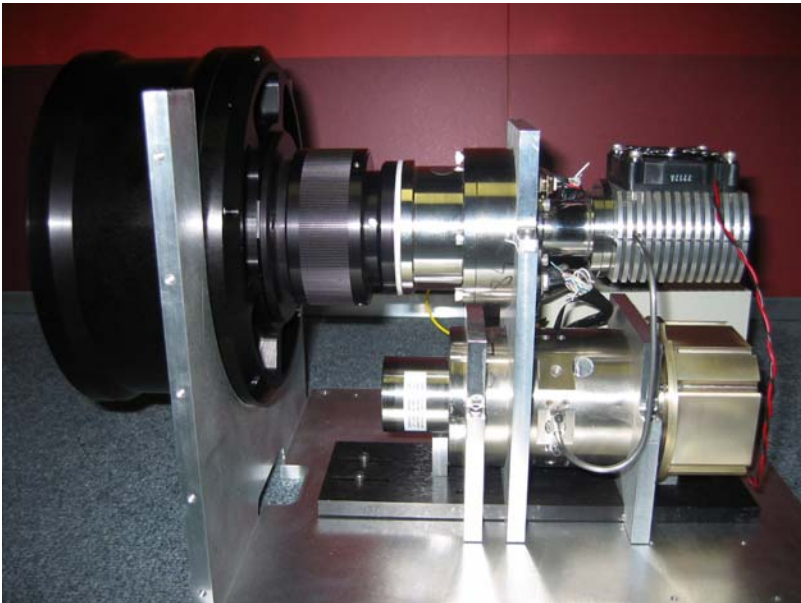


NEDT

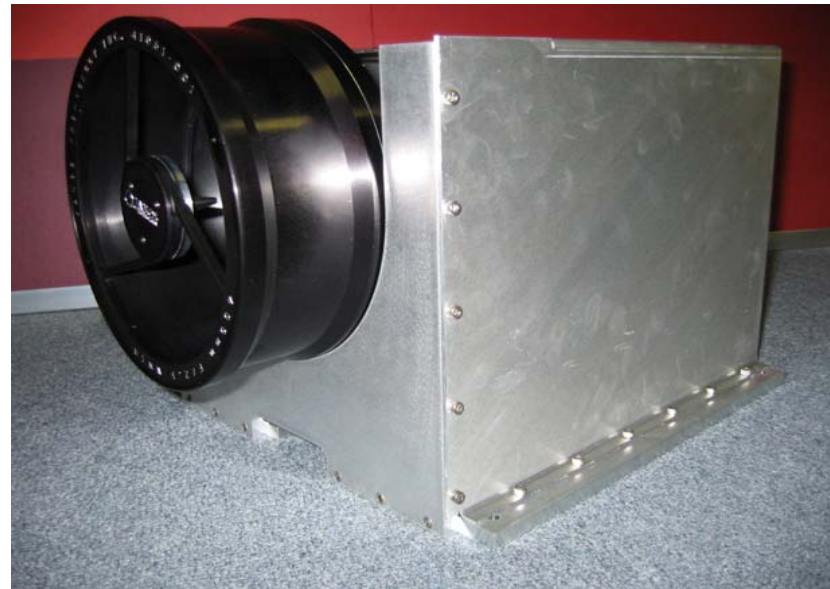


DETECTIVITY

320X256 PIXEL DUALBAND QWIP CAMERA DELIVERED TO THIS APPLICATION



Dualband sensor engine



**320x256 pixel dualband QWIP
camera**

320X256 PIXEL DUALBAND QWIP SPECIFICATIONS

SPECTRAL RANGE	(MWIR)	- 4.4- 5.1 μm (peak 4.7)
PIXEL PITCH		- 40 μm
FILL FACTOR		- 81%
ABSORPTION Q.E.		- 19%
PHOTOCONDUCTIVE GAIN		- 0.2
RESPONSIVITY		- 0.18 A/W
OPERATING TEMP.		- 65 K
NON-U (UNCORRECTED)		- 5%
NON-U (CORRECTED)		- 0.3%
OPERABILITY		- 98%
NEF*		- 7×10^{-16} W/cm ²
SPECTRAL RANGE	(LWIR)	- 8 – 9.1 μm (peak 8.6)
FILL FACTOR		- 86%
PIXEL PITCH		- 40 μm
ABSORPTION Q.E.		- 15%
PHOTOCONDUCTIVE GAIN		- 0.3
RESPONSIVITY		- 0.3 A/W
BLIP TEMPERATURE		- 65 K
NON-U (UNCORRECTED)		- 5%
NON-U (CORRECTED)		- 0.4%
OPERABILITY		- 97.5%
NEF*		- 8×10^{-16} W/cm ²
FRAME RATE		- 30 Hz
OPTICS		- f/2.3; 400 mm & f/2 24 mm

DUALBAND QWIP MOVIE



LWIR

MWIR

Features to look for,

The cigarette lighter produce lots of hot CO₂ gas. So, flare is broader MWIR due to CO₂ emission, where as LWIR (8-9 microns) doesn't have any emission (just the heat).

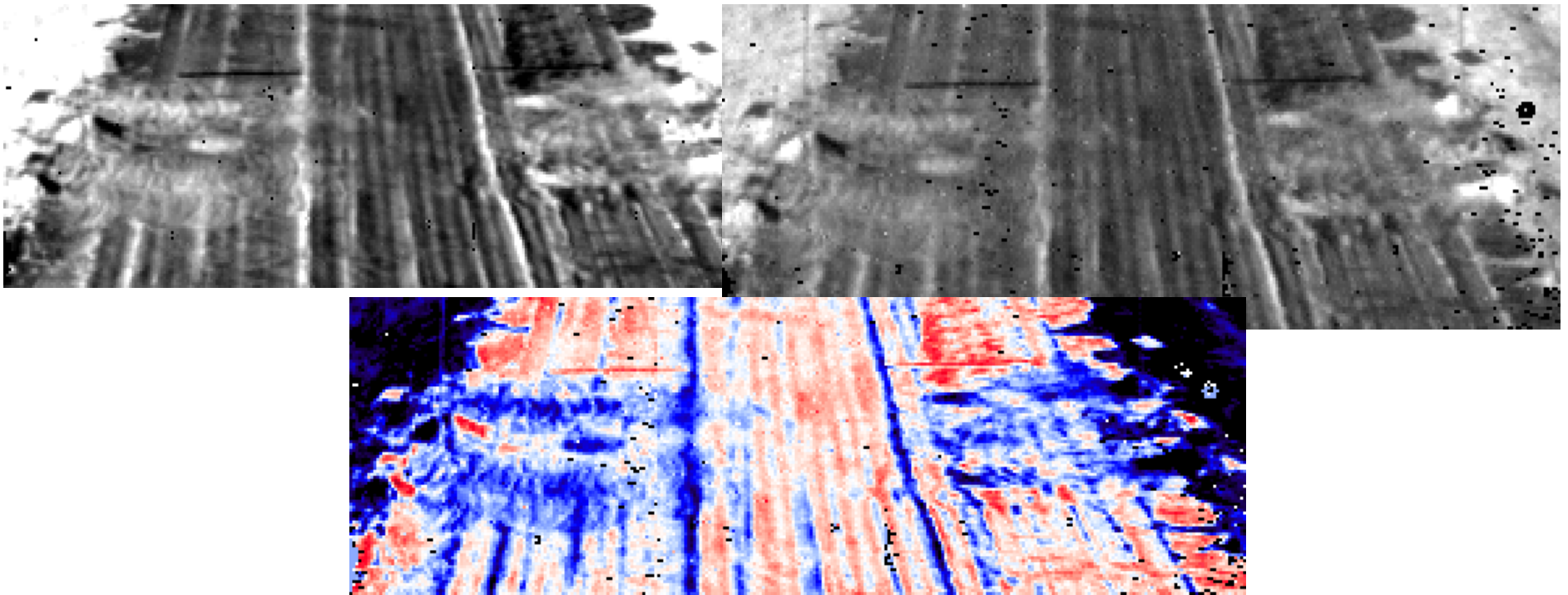
The hot cigarette lighter flame produce so much MWIR signal, it reflects off from the lens and Jason's face.

The plastic piece Jason is holding is opaque in LWIR, but transparent in MWIR.

Format	- 320x256 pixels, dualband & pixel co-registered
Wavebands	- 4.4-5.1 & 8-9 μm
NEDT	- 22 & 24 mK for 300K background with f/2 optics
QE	- 19% & 15%
Photoconductive gain	- 0.2 & 0.3
Detectivity	- $> 2 \times 10^{11}$ & 1×10^{11} Jones
Operating temp.	- 65 K
Fill factor	- $> 81\%$

Mine Detection

- Mine Detection is a current issue that LWIR can answer
- QWIPs are a technology of choice.



1024 x 1024
Two-Color QWIP ROIC :
ISC0501

1024 x 1024 PIXELS DUALBAND ROIC SPECIFICATION

ROIC PARAMETER	SPECIFICATION REQUIREMENT	COMMENTS
Array Configuration	1024 x 1024	Large-format
Pixel Size	30um x 30um	
Spectral Range	MWIR: 4.3-5.1um (Color A) LWIR: 8-9um (Color B)	Drives well capacity requirements
Input Polarity	Hole Collection	GaAs/AlGaAs QWIP detector
Input Configuration	Direct Injection (DI)	P-Channel Inputs
Input Clock Rise and Fall	CLK: 10ns rise/fall FSYNC, DATA: 10ns rise/fall	10% to 90%
Number of Outputs	8 Analog per color	Additional 1 reference output/Color Analog at 10MHz (8/Color+1Ref/Color=18 outputs total)
Output Modes	4, and 8 Analog per color	Common Output Mode for each color
Windowing	Row Only Windowing Minimum Window of 1 Rows	
Frame Rate (1024 x 1024)	60Hz (8 outputs per color)	ITR, IWR, Additional 1 reference output/color
Total Well Capacity	$\geq 17 \times 10^6$ carriers	Unit Cell Layout Limited, Goal of 20×10^6 carriers
Well Capacity Ratio	4:1 (LWIR:MWIR)	$\pm 10\%$, Repartition can be accomplished with 1-3 layer mask change
Noise	$\leq 420 e^-_{RMS}$ at $3.4 \times 10^6 e^-$ $\leq 1250 e^-_{RMS}$ at $13.6 \times 10^6 e^-$	MWIR (Color A) LWIR (Color B)
Power	$\leq 600mW$	8 Output Mode with No Output reference, Goal of $\leq 400mW$

SUMMARY

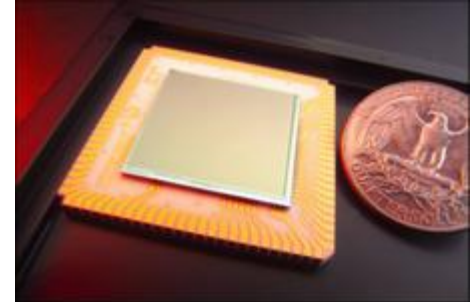
- Demonstrated 1024x1024 pixel MWIR & LWIR focal plane arrays.
- Demonstrated 320x256 pixel MWIR/LWIR pixel collocated focal plane array.
- Increased QE from 19% to 36%. We will incorporate high QE material with dualband QWIPs.

Long-Wavelength Infrared (LWIR) Quantum Dot Infrared Photodetector (QDIP) Focal Plane Array

Motivation for Quantum Dot Based LWIR FPAs

✓ Build on the advantages of QWIP FPAs

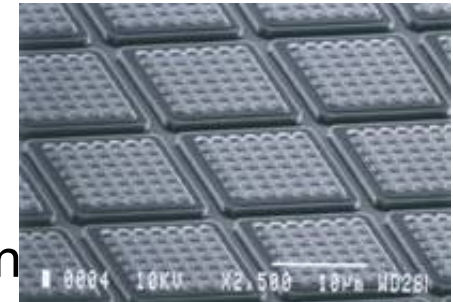
- Large format
- Excellent uniformity
- Excellent operability
- Low $1/f$ noise
- Thinned arrays eliminate
 - Optical crosstalk
 - Thermal mismatch with ROIC
 - Pixel delamination



1024x1024 MWIR FPA
Designed, grown, and fabricated at JPL

+ Add quantum dot capabilities

- Normal incidence absorption
- Higher temperature operation (lower dark current)
- Higher responsivity (longer lifetime)
- Further increase the radiation hardness



Individual pixels in an FPA, with
integrated grating structure

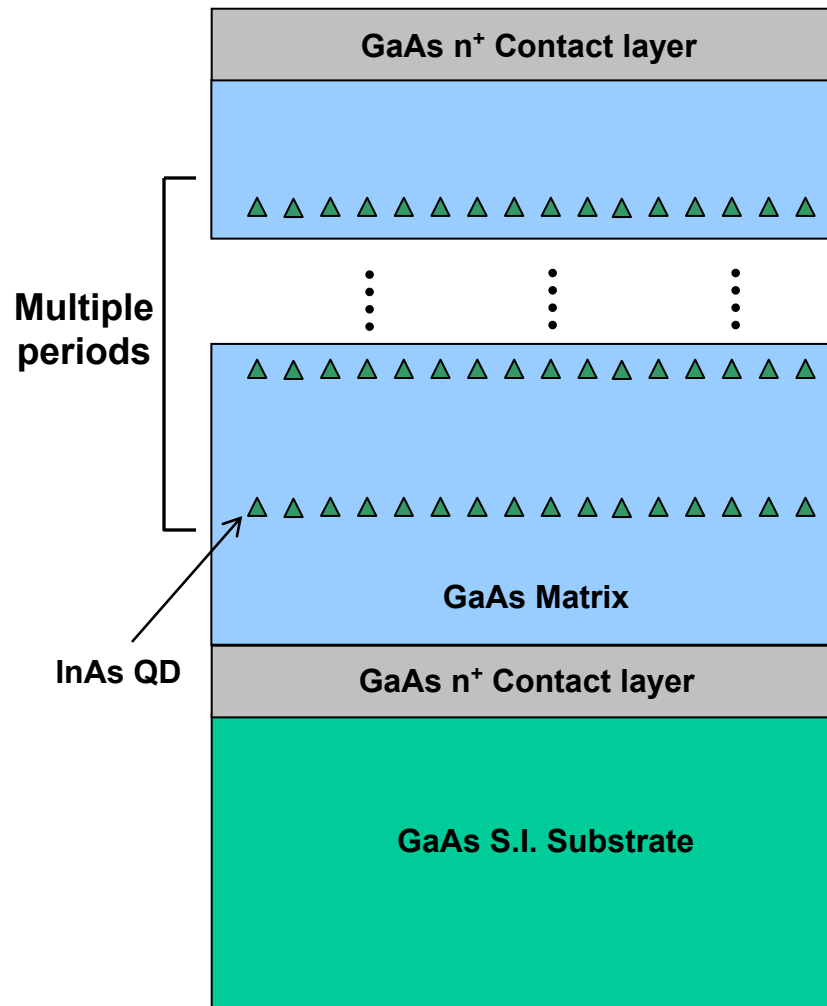
= **New generation of high performance high operating temperature infrared focal plane arrays**

Outline

- Initial Device Development
- Focal Plane Array Development
- Improved quantum efficiency devices
- Summary

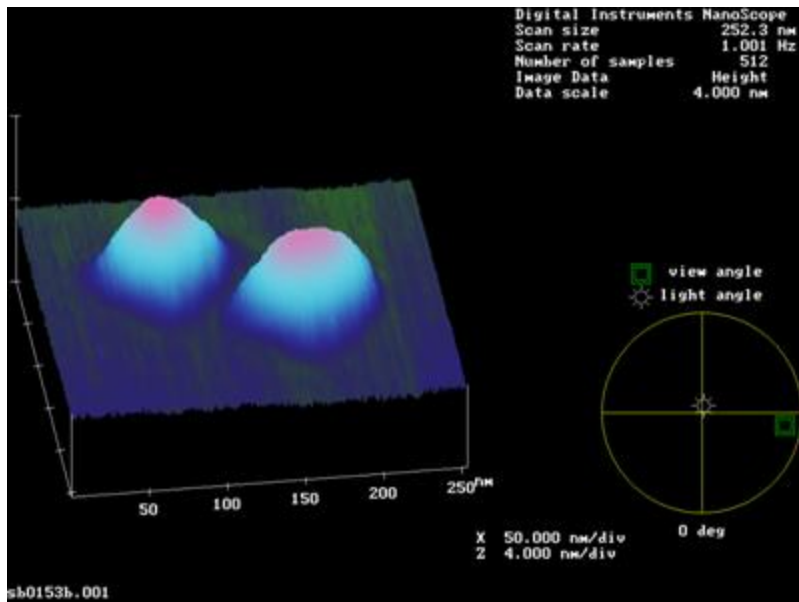
Initial Device Development

Quantum Dot Infrared Photodetectors (QDIPs)



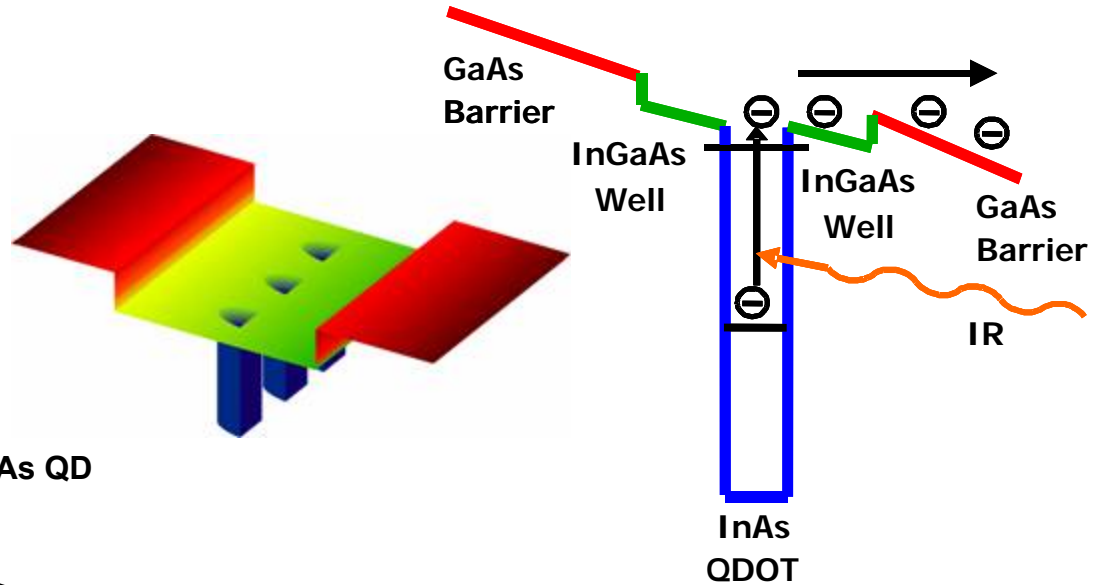
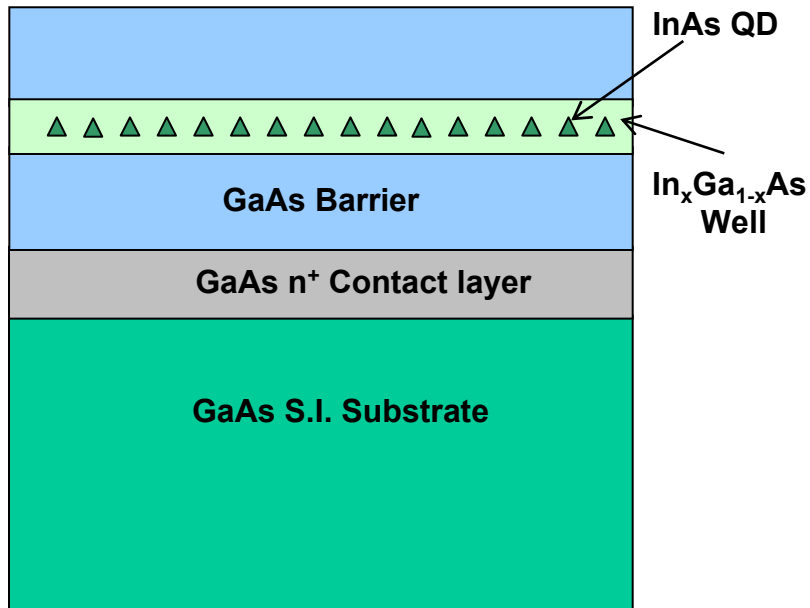
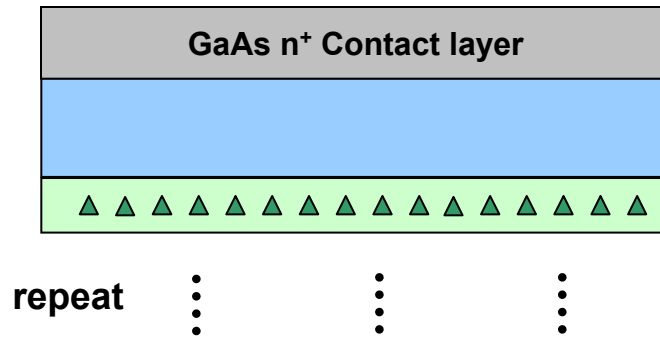
- InAs quantum dots (QDs) embedded in GaAs matrix
- Quantum dots act as infrared absorbers
- Dot size and doping adjusted for optimum response
- Multiple stacks of QD layers grown to boost quantum efficiency
- Photoconductor
 - Unipolar device, n⁺ contacts.

Quantum Dot Growth



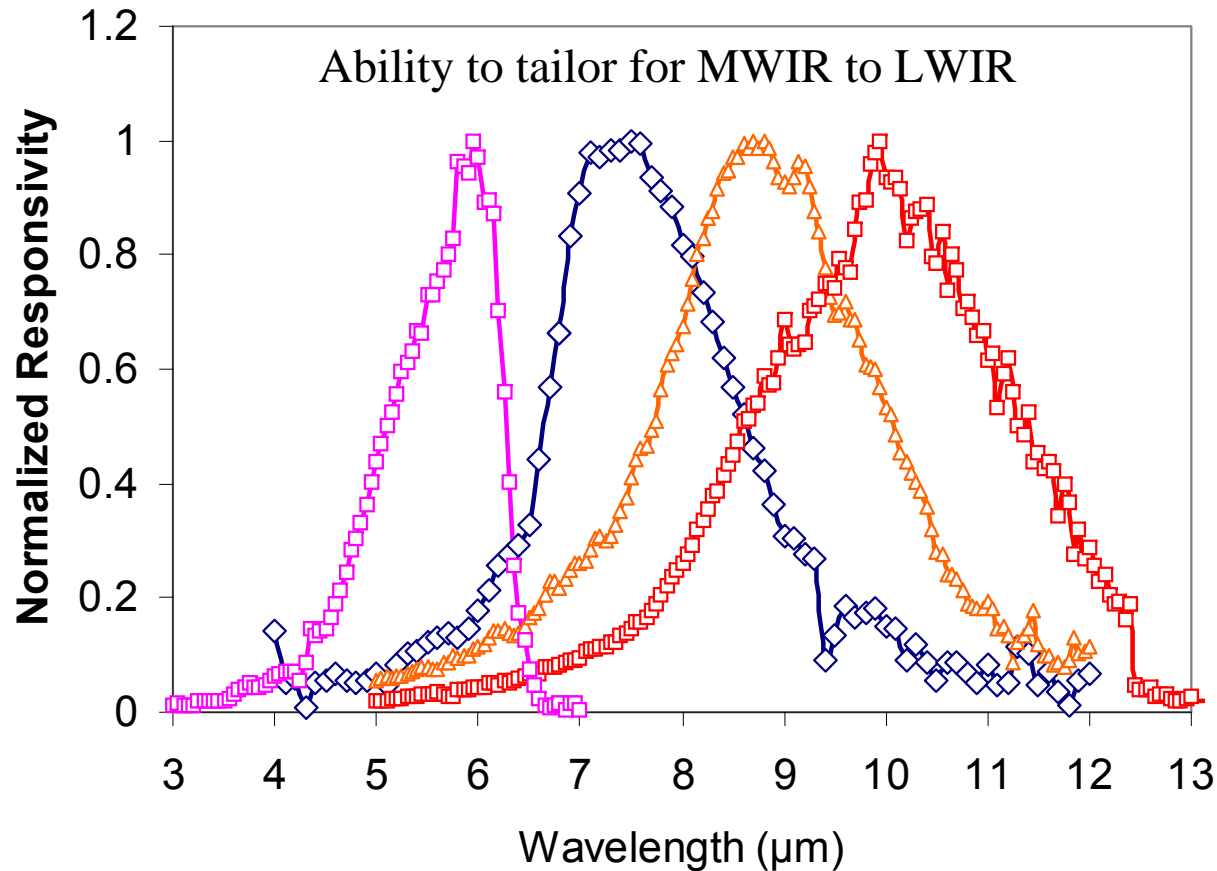
- Grown in JPL's Veeco Gen III Molecular Beam Epitaxy (MBE) machine (4 inch capable)
- Quantum dots formed by a self-assembly process
 - Deposition of semiconductor on lattice-mismatched substrate
- InAs and InGaAs dots on GaAs substrates

Dot-in-the-Well (DWELL) QDIP



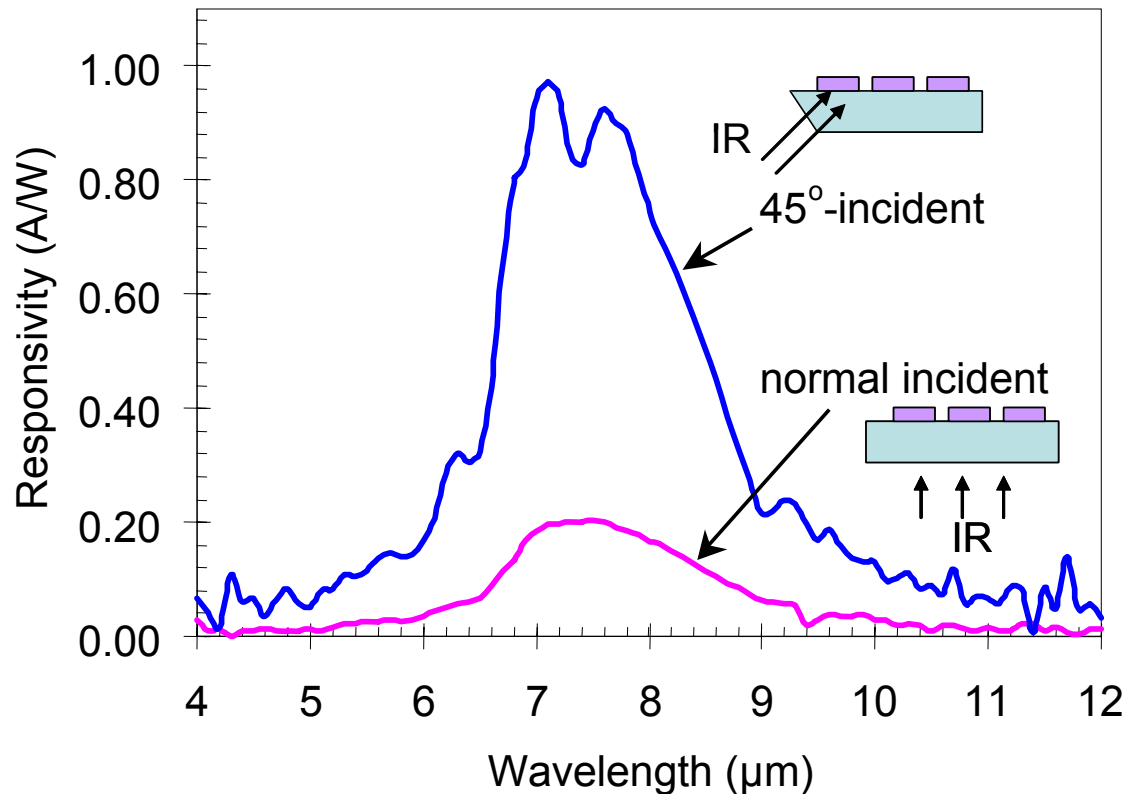
- Embed InAs dots in InGaAs quantum wells
- Motivation: Precise control of quantum well width enables easier **wavelength tuning**

Wavelength Tuning in DWELL QDIP



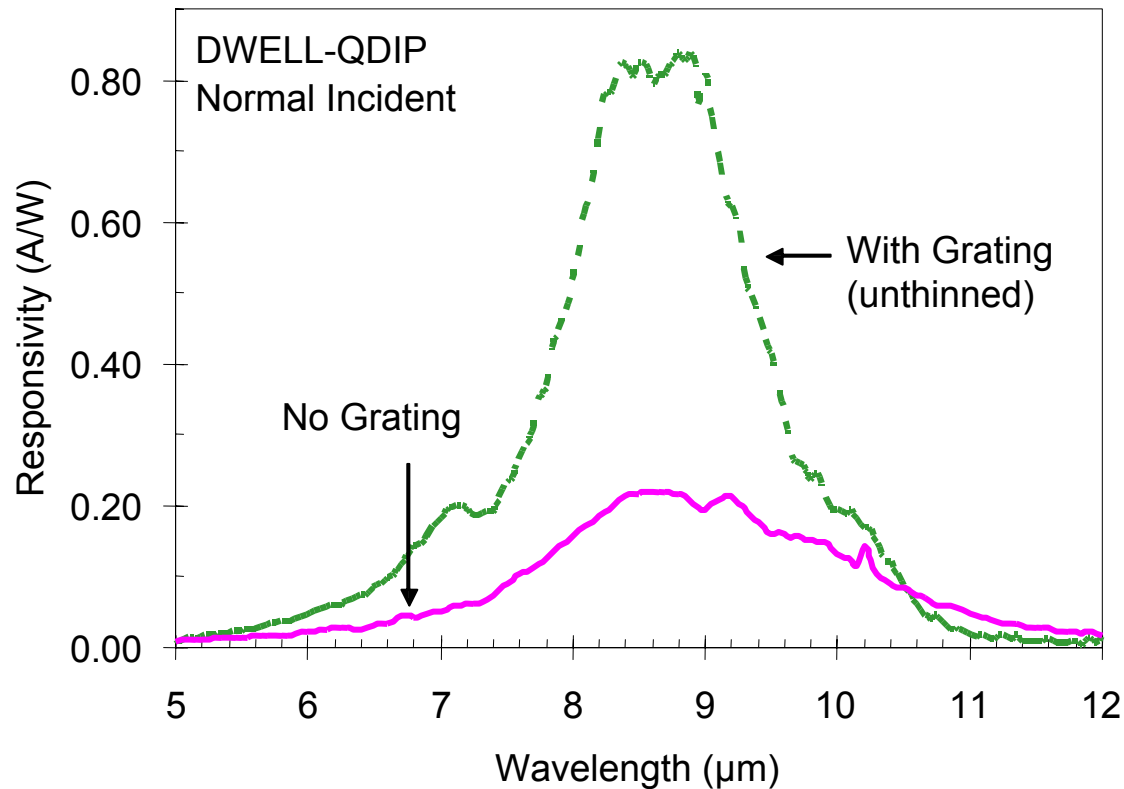
- Experimentally measured spectral responsivity of DWELL QDIP
- Continuous spectral tunability via well width variation

Normal and 45° Incidence Response



- Much stronger normal incidence response as compared to quantum well infrared photodetectors (QWIPs)
- 45° incidence yields even stronger response
- Consistent with theoretical modeling results

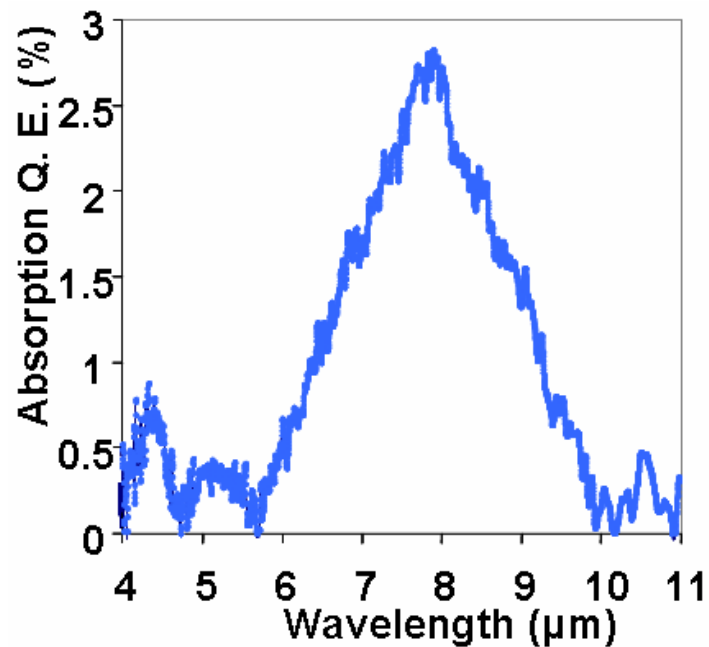
Grating Enhancement



- Observation of strong 45° incidence response led to implementation of reflection grating
- Normal incidence response now significantly enhanced by grating

Internal Quantum Efficiency

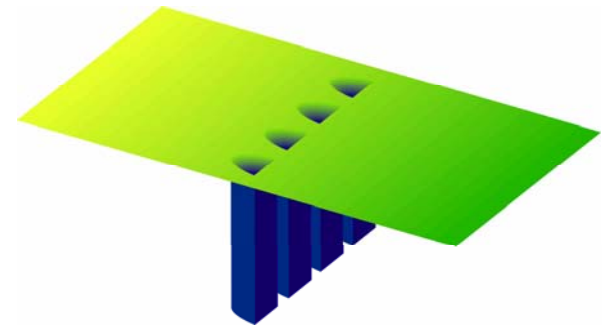
- QDIPs typically have low QE. Prior published reports of QDIP QE in literature with QE at 0.1%.
- Internal QE of 0.67% was obtained for the initial DWELL-QDIP device through noise measurement



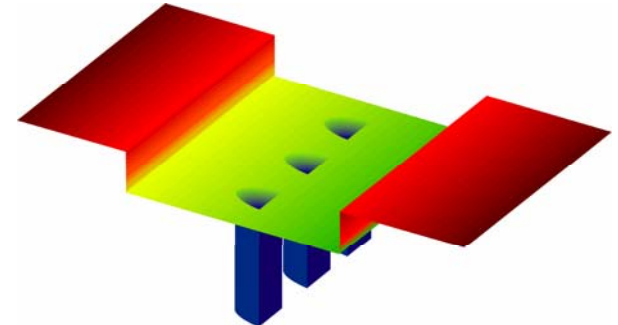
- Subsequent material improvement yielded QE= 2.8% through FTIR absorption measurement

Quantum Efficiency and Gain

- Conventional QDIPs have low QE and high gain
 - $g=823$, $\eta=0.02\%$, *Appl. Phys. Lett.* **84**, 2166 (2004)
 - $g\sim 1000$, $\eta\sim 0.1\%$, *Nanotech.* **16**, 219 (2005)
 - High gain due to polaron-relaxation related long carrier lifetime
- Dot-in-the-well QDIPs have smaller gain
 - Carriers trapped by quantum wells
- DWELL QDIPs have higher QE
 - Higher electron concentration near dots
 - More rapid refilling of QD ground state
 - Possibly leading to higher QE
- Can engineer trade-off between QE and gain
 - Note BLIP D^* depends on absorption QE, independent of gain

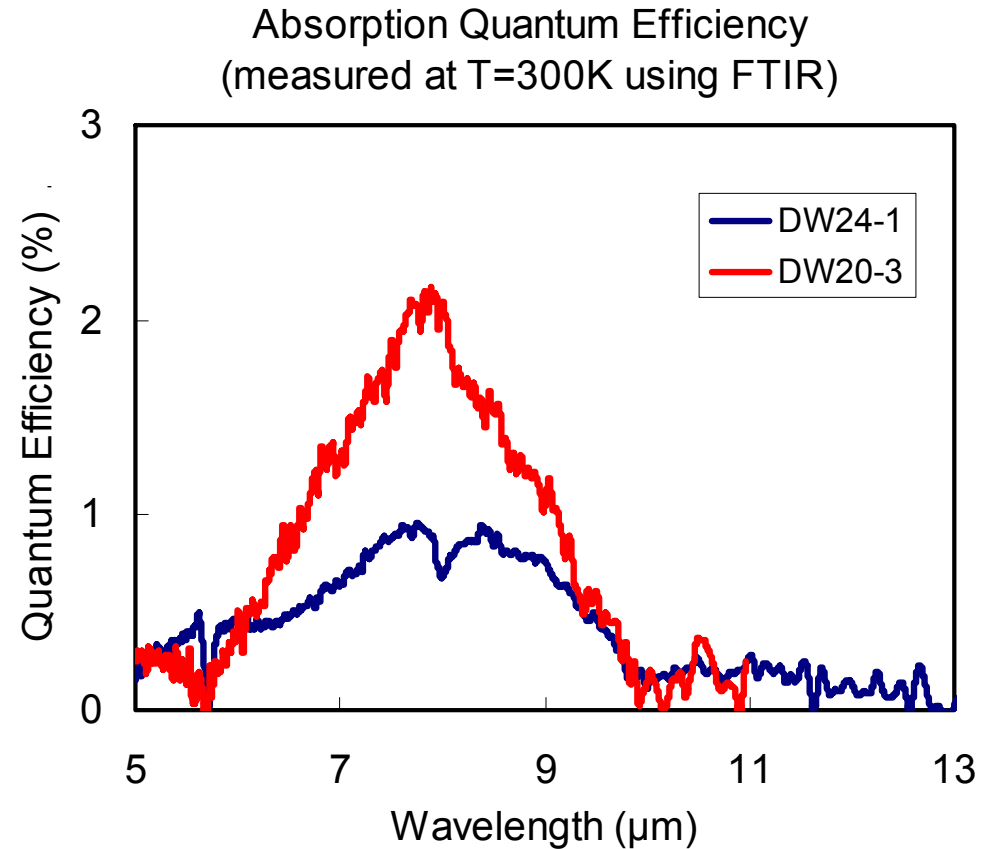
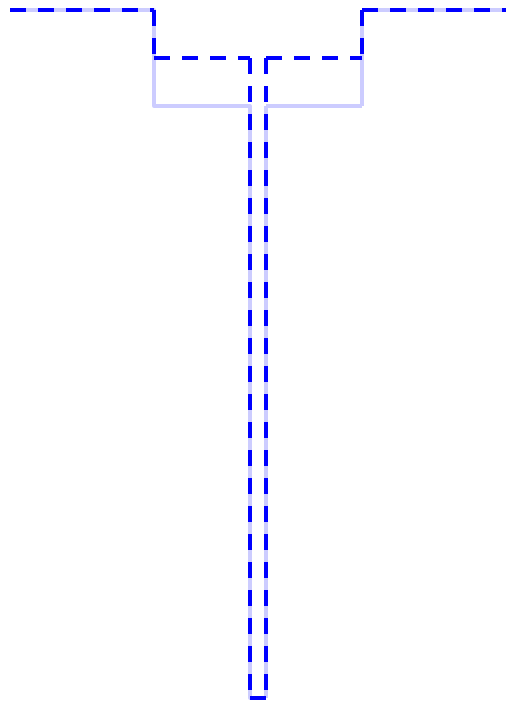


Conventional QDIP



DWELL QDIP

QE and Gain Trade-Off in DWELL QDIP

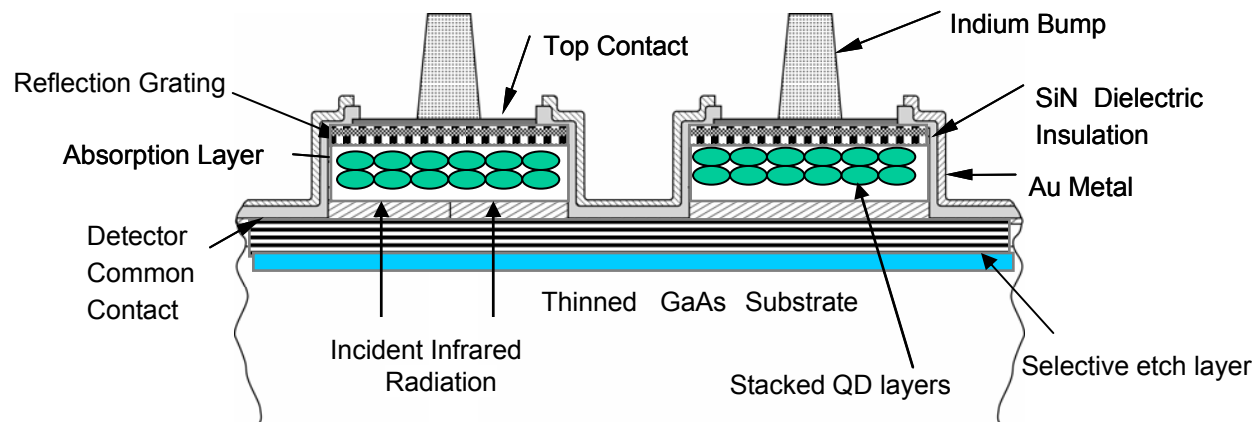


- DW24-1 has a shallower quantum well: $g=2.4$, QE=1.2% (77K)
- DW20-3 has a deeper quantum well: $g=0.4$, QE=2.8% (77K)

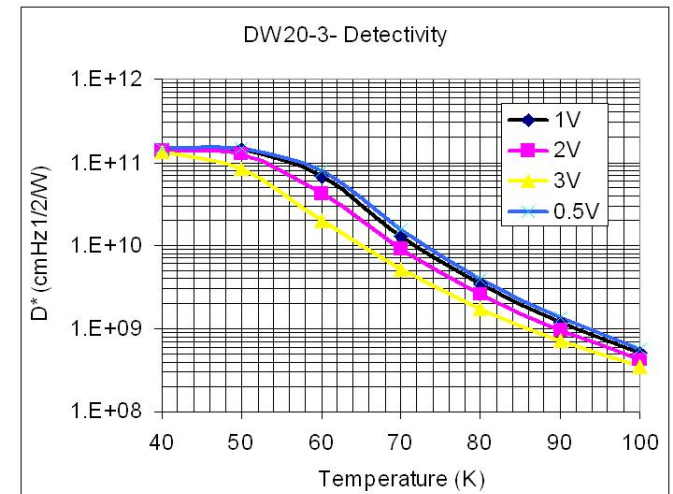
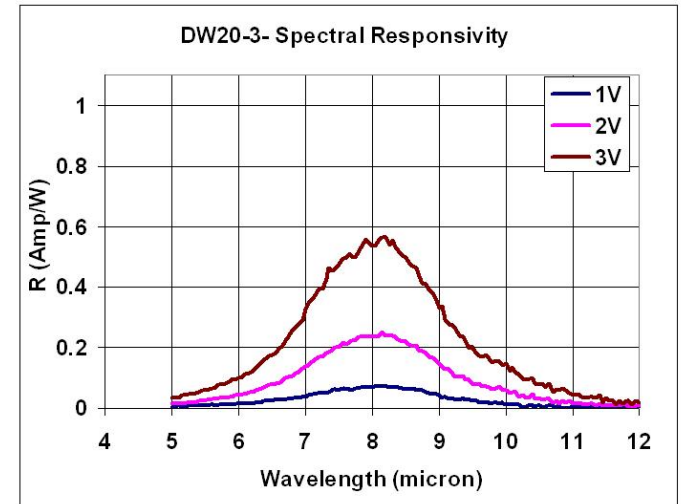
Quantum Dot Infrared Focal Plane Array Development

Focal Plane Array

- Originally proposed a small 32x32 test array
- Detector: 30-stack InAs Q-dots embedded in InGaAs/GaAs quantum wells; doping=2 e per dot; single device QE=2.8%
- Integrated reflection grating structure
- 640x512; 25 μm pixel pitch (23 μm pixel width)
- ROIC:
 - direct injection, well capacity 11 million electrons



Infrared Imaging



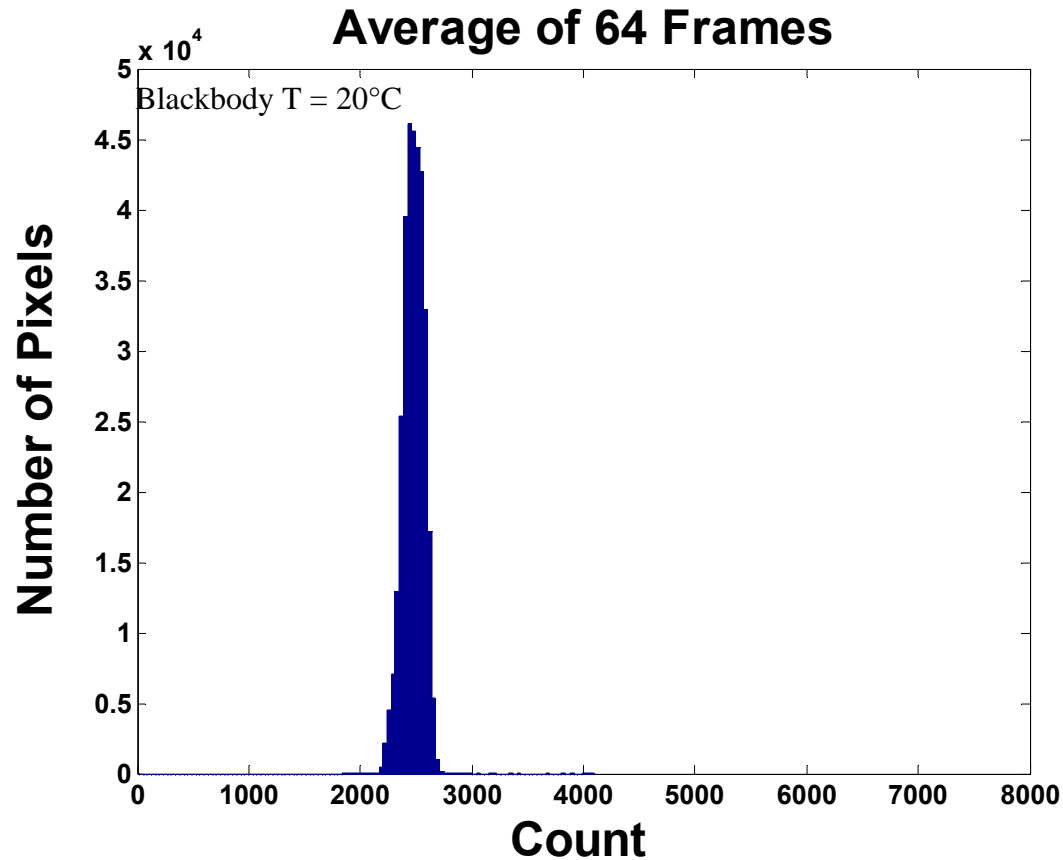
- 640x512 image taken at 60 K using f/2 optics
- Non-uniformity <0.2% (corrected); >99% operability; NEDT = 40 mK

FPA Performance - Imaging



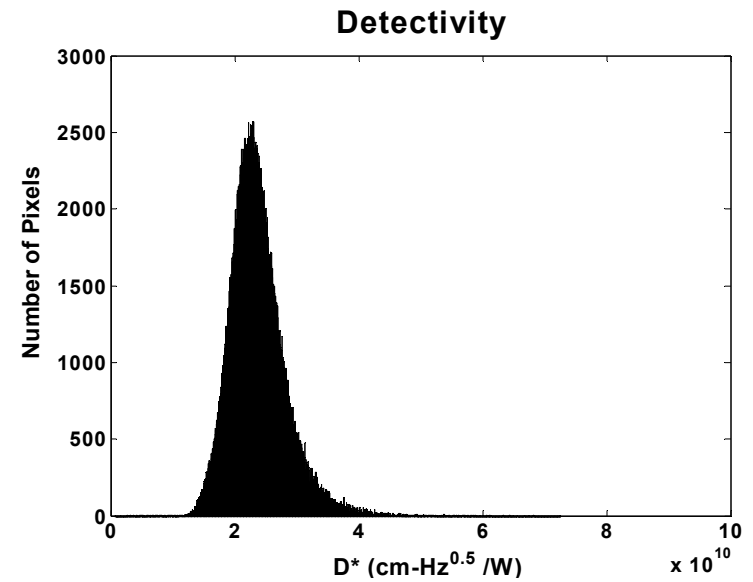
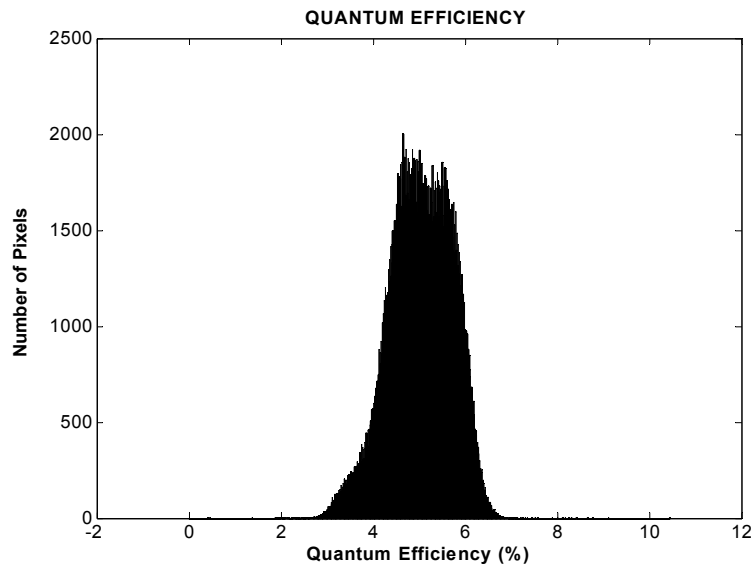
- 640x512 image taken at 60K using f/2 optics

FPA Uniformity

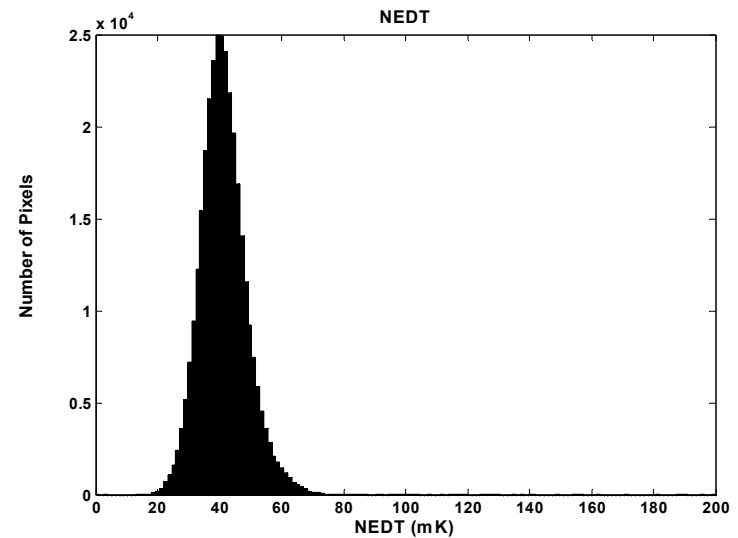


- Uncorrected nonuniformity < 6.7%
- Corrected nonuniformity < 0.2%
- Operability > 99%

FPA Figures of Merit

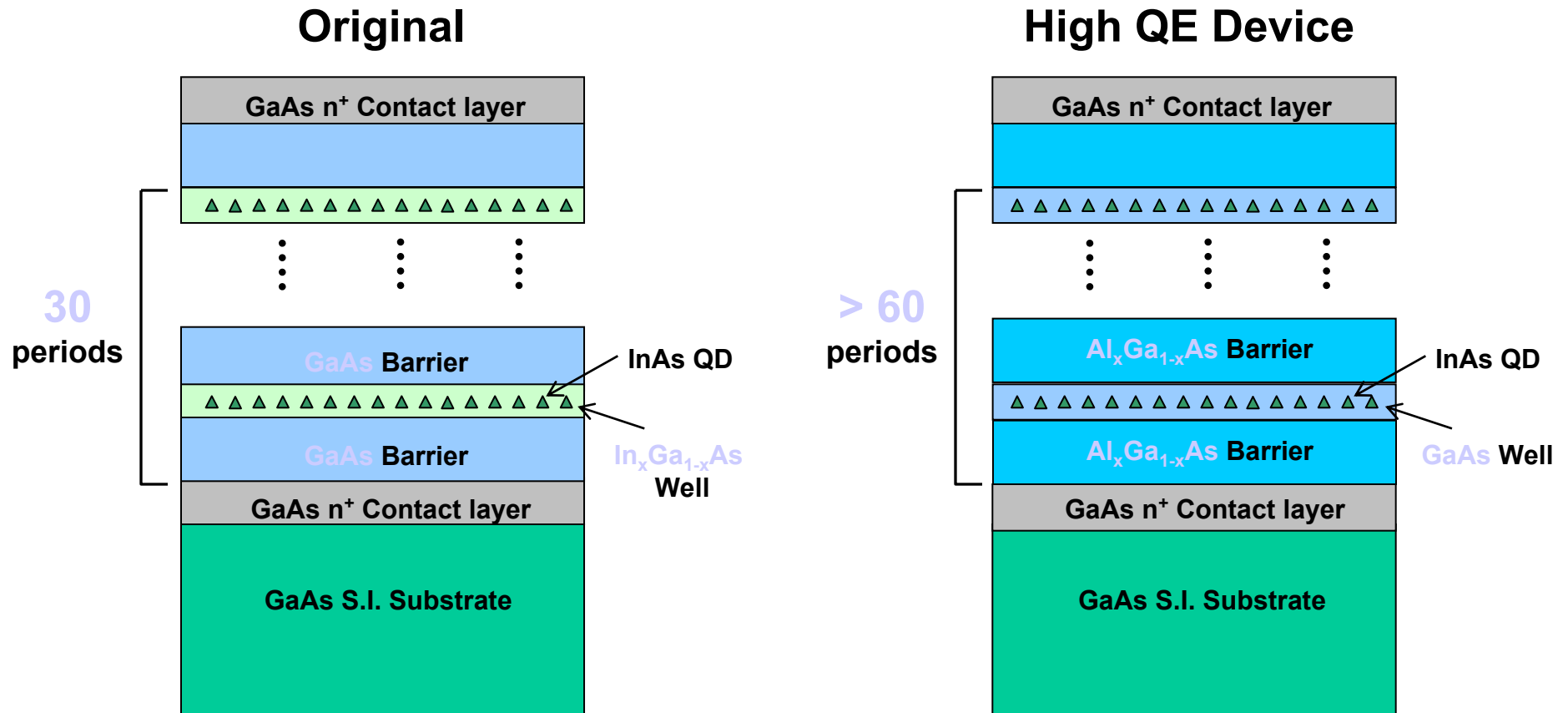


Wavelength	- 9 μm
Array Size	- 640x512
Pixel Pitch	- 25 μm
Quantum Efficiency	- 5%
Detectivity	- 2×10^{10} Jones
NE Δ T	- 40 mK



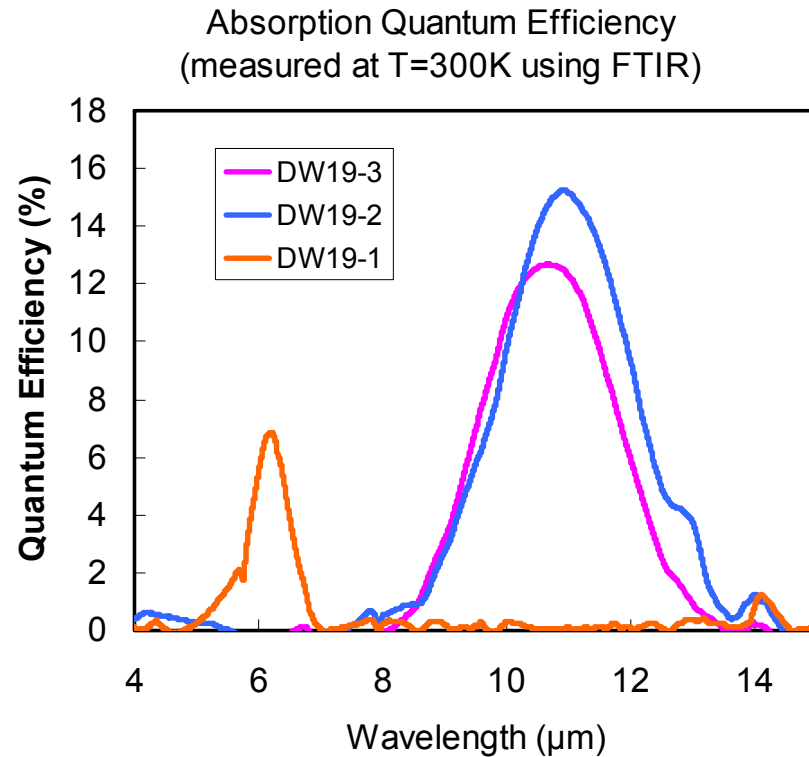
Improved Quantum Efficiency Quantum Dot Infrared Photodetectors

Improved QE Device with Enhanced Normal Incidence Absorption



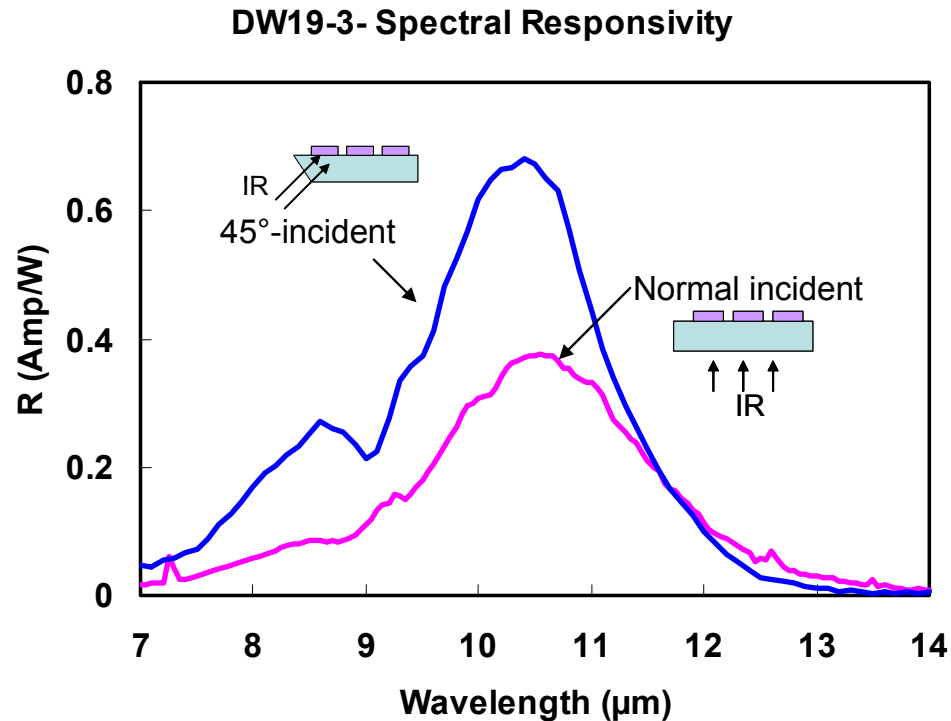
- Replaced InGaAs/GaAs with superior GaAs/AlGaAs quantum wells
- Less overall strain; **more quantum dot stacks**
- Improved doping profile in quantum well/dot region

Improved QE Device Performance



- Highest QE measured in QDIPs
 - DW 19-1, 40 QD stacks; DW19-2, DW19-3, 60 QD stacks
- First set of quantum dots in GaAs/AlGaAs wells are far from optimized but are yielding best D^* among our DWELL devices

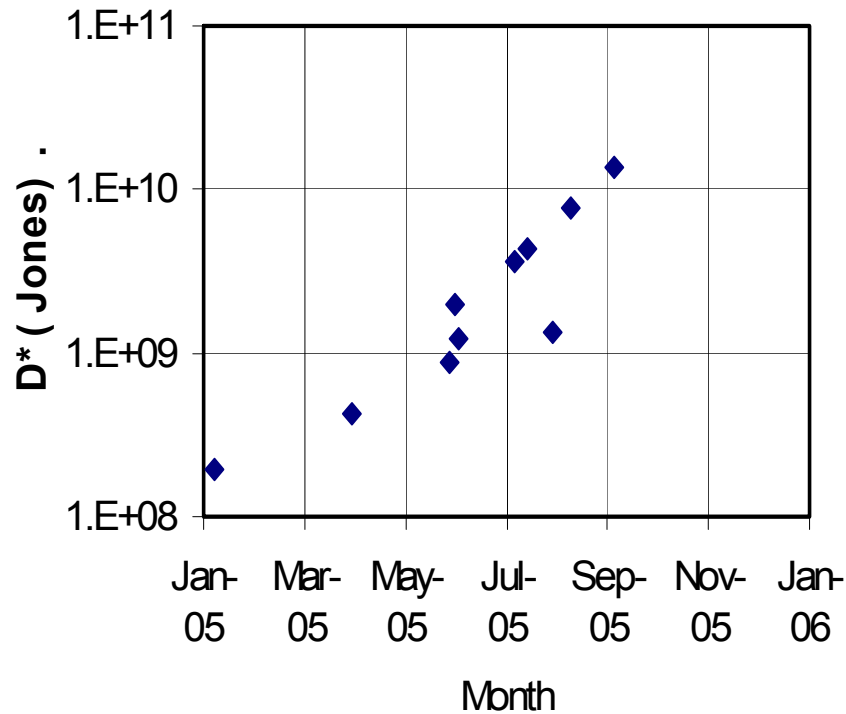
QDIP Exhibits High Normal Incidence



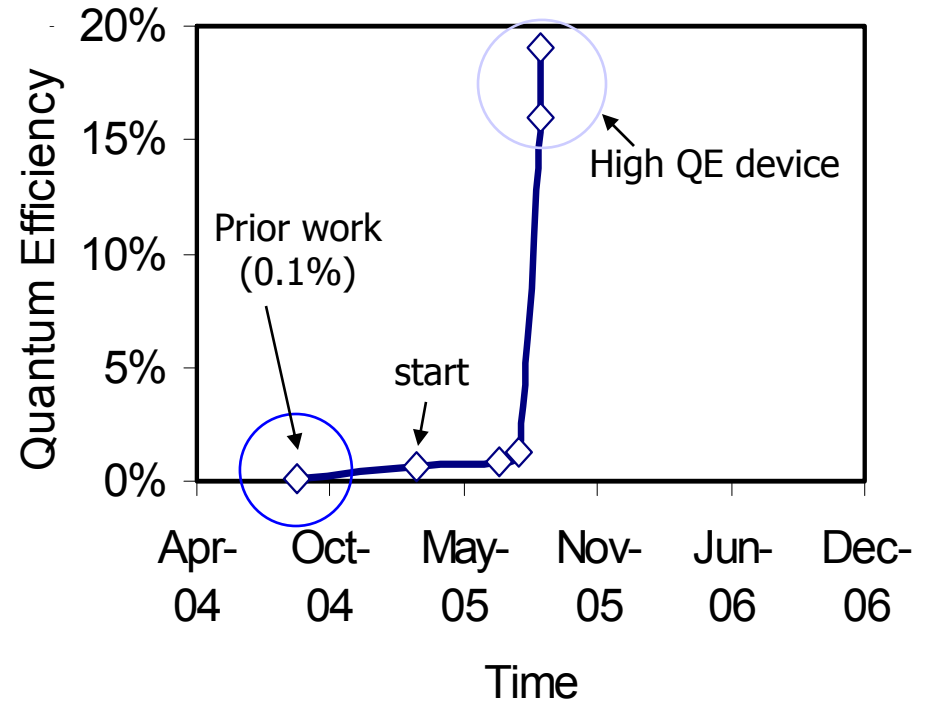
- Highest normal incidence response we have seen in a intersubband IR detector
- Expect further normal incidence response enhancement through integration of an optical reflection grating

Rapid Progress

Progress of LWIR DWELL-QDIP Detectivity
(T=77K, scaled to 10 μm detector)



Quantum Efficiency at T = 77K



- Significant improvements in D^* and QE
 - D^* normalized to 10 μm for ease of comparison

Summary

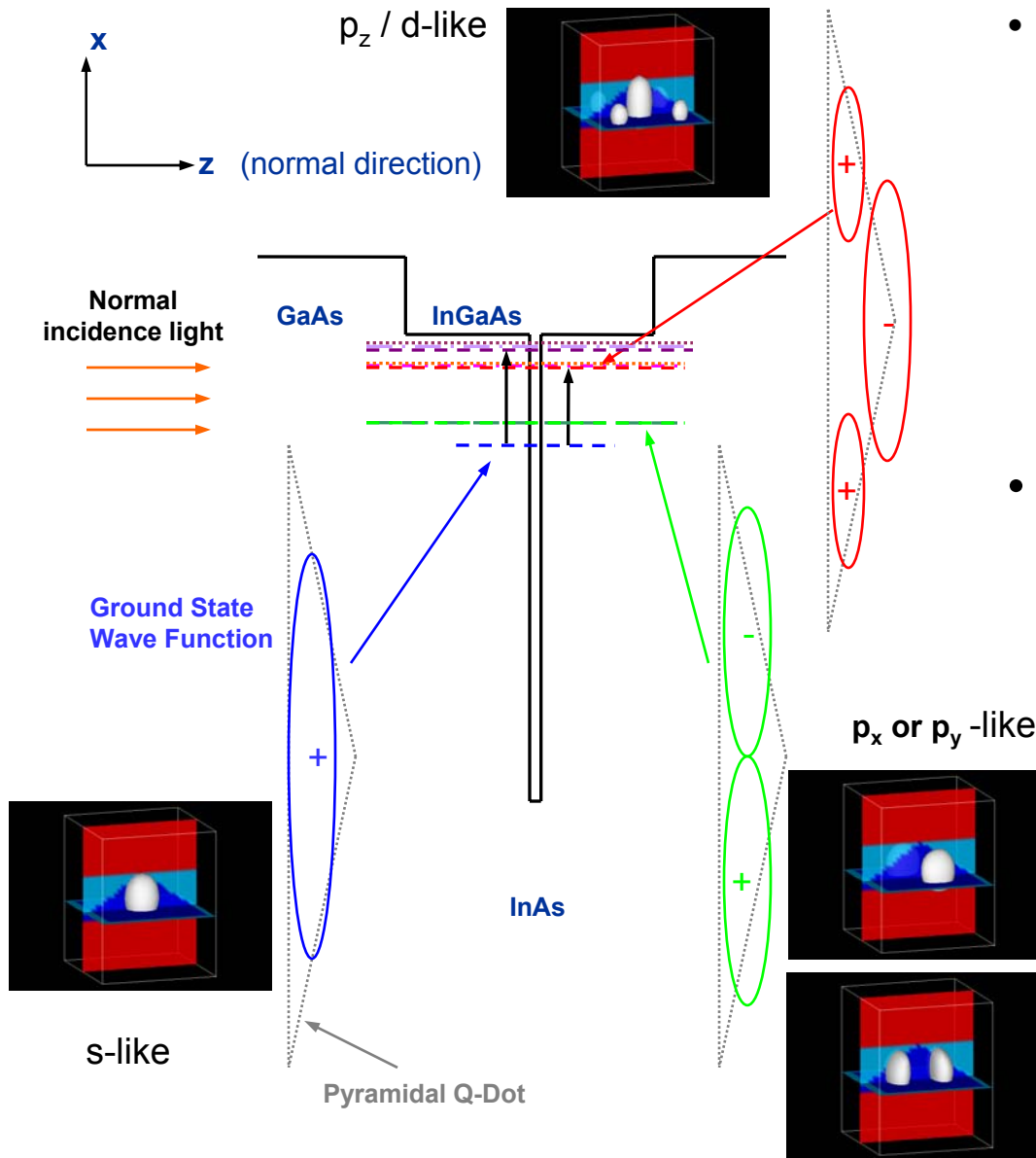
- QDIP Device Development
 - demonstrated high normal and 45° incidence responsivity
 - demonstrated utility of using an integrated reflection grating
- Highest quantum efficiency (QE) obtained in a quantum dot infrared photodetector (QDIP)
 - Demonstrated 16% absorption QE
 - Demonstrated the possibility of achieving improved QE over QWIP
- Demonstrated that QDIP FPA retains the uniformity advantages of QWIP FPA
 - Large-format (640x512) QDIP based FPA
 - High operability (>99%)
 - Low non-uniformity (< 0.2% corrected)
 - Low NE Δ T (40 mK@ 60K)

Quantum Well and Quantum Dot Modeling

Motivation and Approach

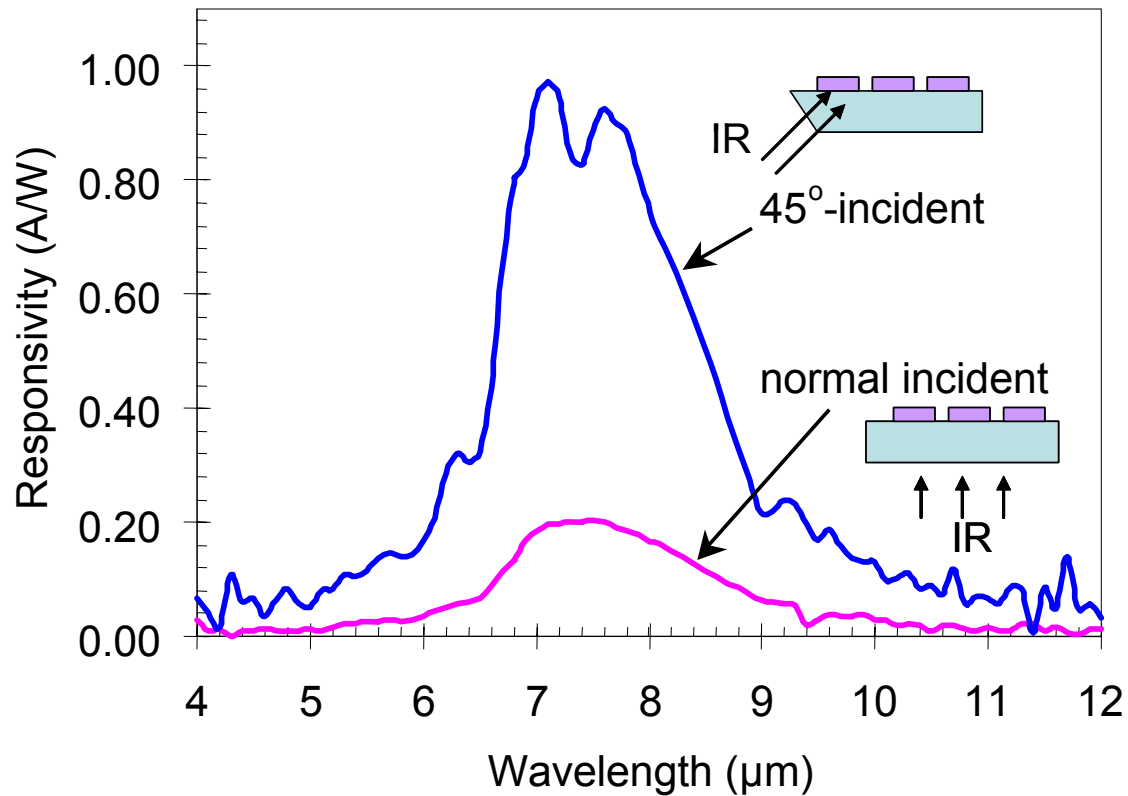
- Experimentally measured photoresponse of an InAs/InGaAs/GaAs dot-in-the-well (DWELL) structure shows normal incidence response can be a sizeable fraction of the 45° incidence response.
- Experimentally measured photoresponse of an AlGaAs/GaAs/AlGaAs QWIP structure shows sizeable background absorption at long wavelengths ($>10 \mu\text{m}$)
- Explore this physical phenomenon by theoretical investigation (14-band model + impurity) for possible explanations.

Photoresponse in DWELL Structure



- The fundamental transition (ground to p_x or p_y like states) yields no appreciable photocurrent.
 - Very strong normal incidence absorption.
 - But upper state is deeply bound
- Observed photocurrent is attributed to transitions from the **s-like** ground state to states in the p_z - or d- like and higher states.
 - Predominantly z-polarization absorption. (QWIP-like; can activate with grating)
 - Also has weaker x,y-polarization (normal incidence) absorption.

Normal and 45° Incidence Response in Dot-in-the Well Structure



- 45° incidence yields stronger response
- Relative to the 45° response, the normal incidence response is much stronger than in QWIPs
- Similar behavior seen in QDIPs

Observation and Possible Explanations

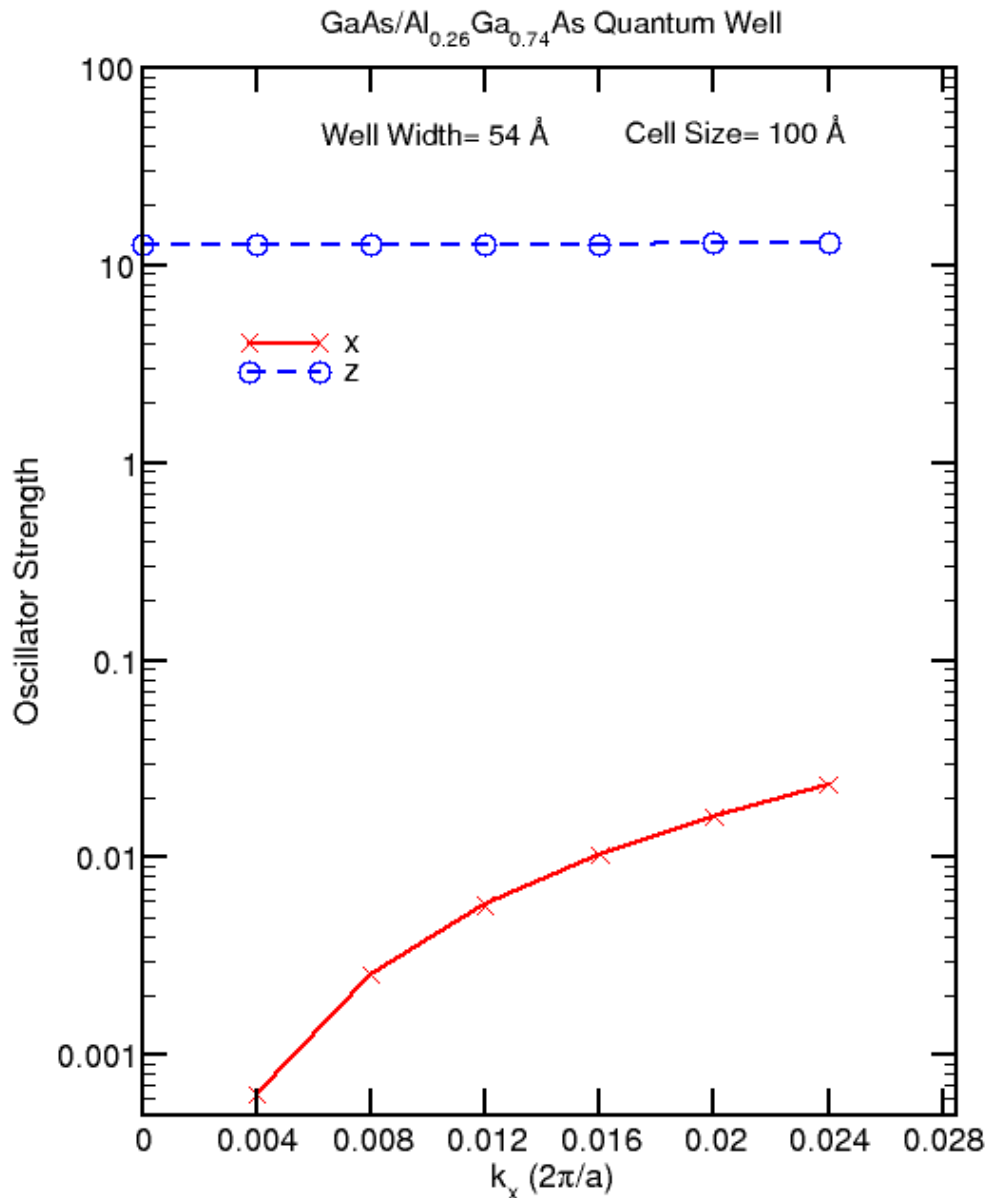
- Relatively strong normal incidence response observed experimentally
- Simple effective mass model predicts no normal incidence oscillator strength for transitions from s-like ground state to p_z like states.
- Possible Explanations:
 - Band structure effects (due to mixing with other bands)
 - Impurity scattering Effects
 - Dopant hydrogenic wave function radius can be comparable to size of quantum dot
 - Transition to higher states
- Investigate theoretically

Theoretical Analysis

- Energy and wave functions computed using a stabilized transfer matrix technique by dividing the system into many slices along growth direction.
- Envelope function approximation with energy-dependent effective mass is used.
- Effective-mass Hamiltonian in k-space:
$$[(k_x^2+k_y^2)/m_t(E)+\partial_z^2/m_l(E)-E]F(\mathbf{k}) + \sum_{\mathbf{k}'}[V(\mathbf{k},\mathbf{k}')+V_{imp}(\mathbf{k},\mathbf{k}')]F(\mathbf{k}')=0$$
is solved via plane-wave expansion in each slice.
- 14-band k·p effects included perturbatively in optical matrix elements calculation
- Dopant effects incorporated as screened Coulomb potential
- The technique applies to quantum wells and quantum dots (or any 2D periodic nanostructures)

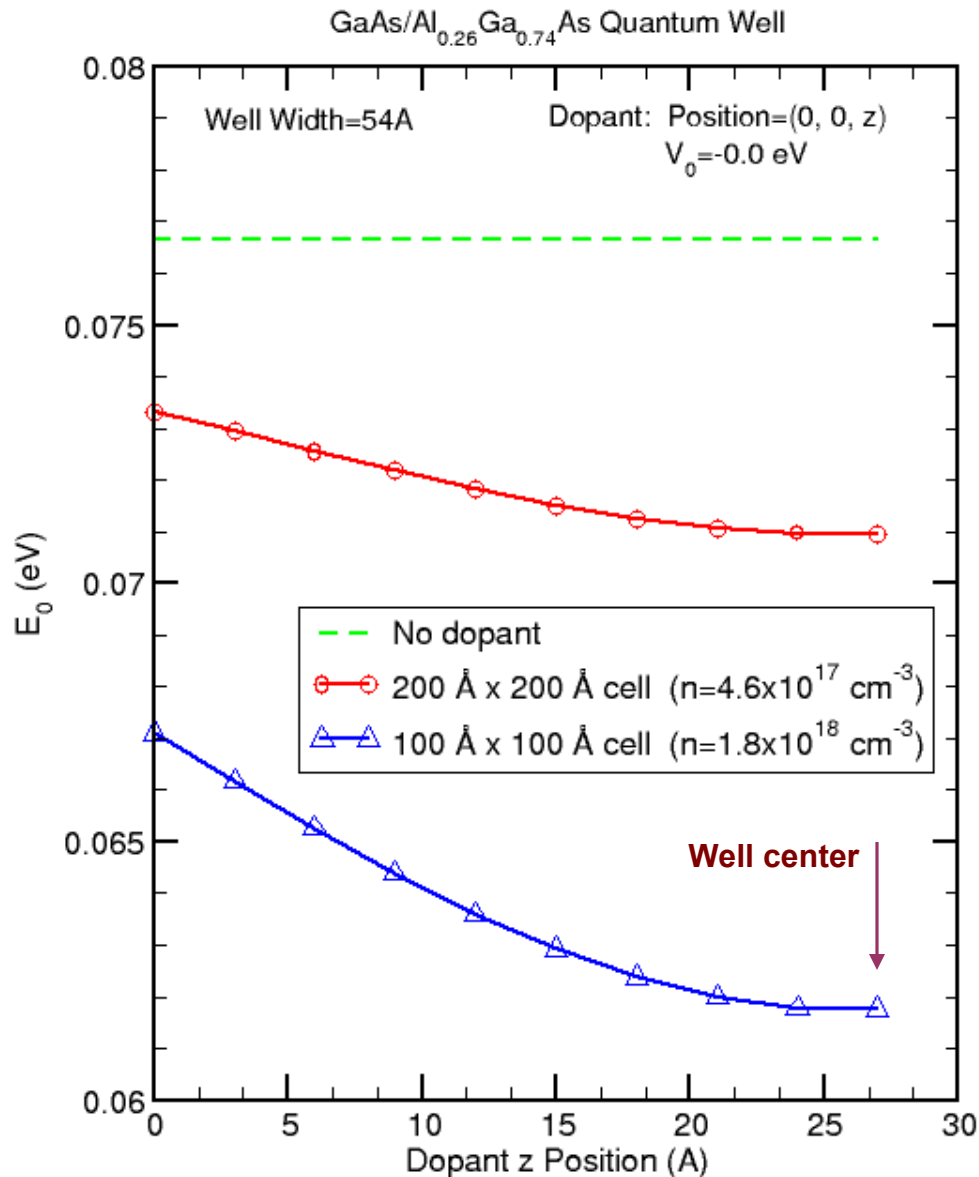
Quantum Well

Band Structure Effect on Oscillator Strengths



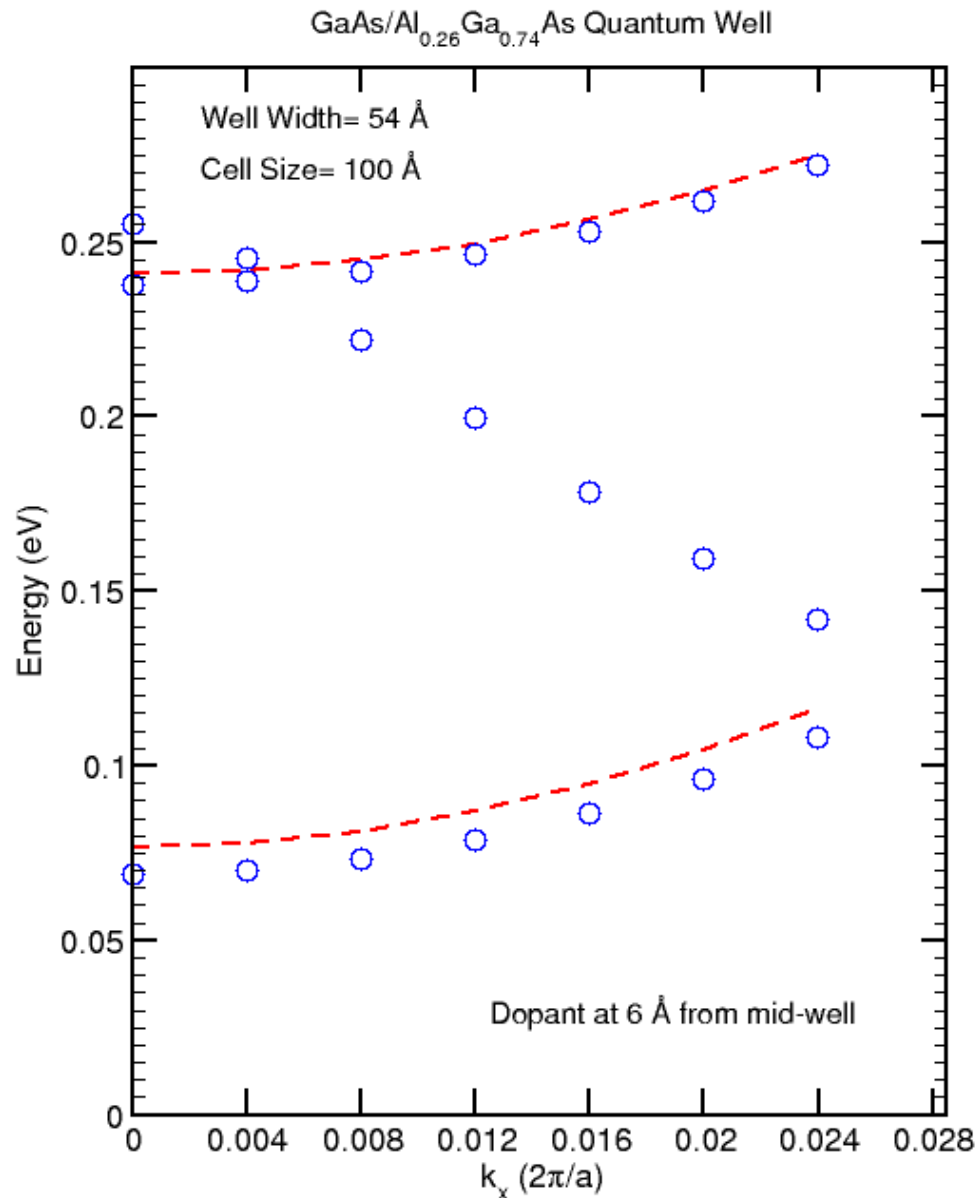
- GaAs/Al_{0.26}Ga_{0.74}As quantum well
 - 54 Å wide GaAs well
- Band structure effect predicts > 0.2% x to z oscillator strengths ratio at $k_x=0.02$
- In general agreement with results reported in the literature

Ground State Energy with Impurity



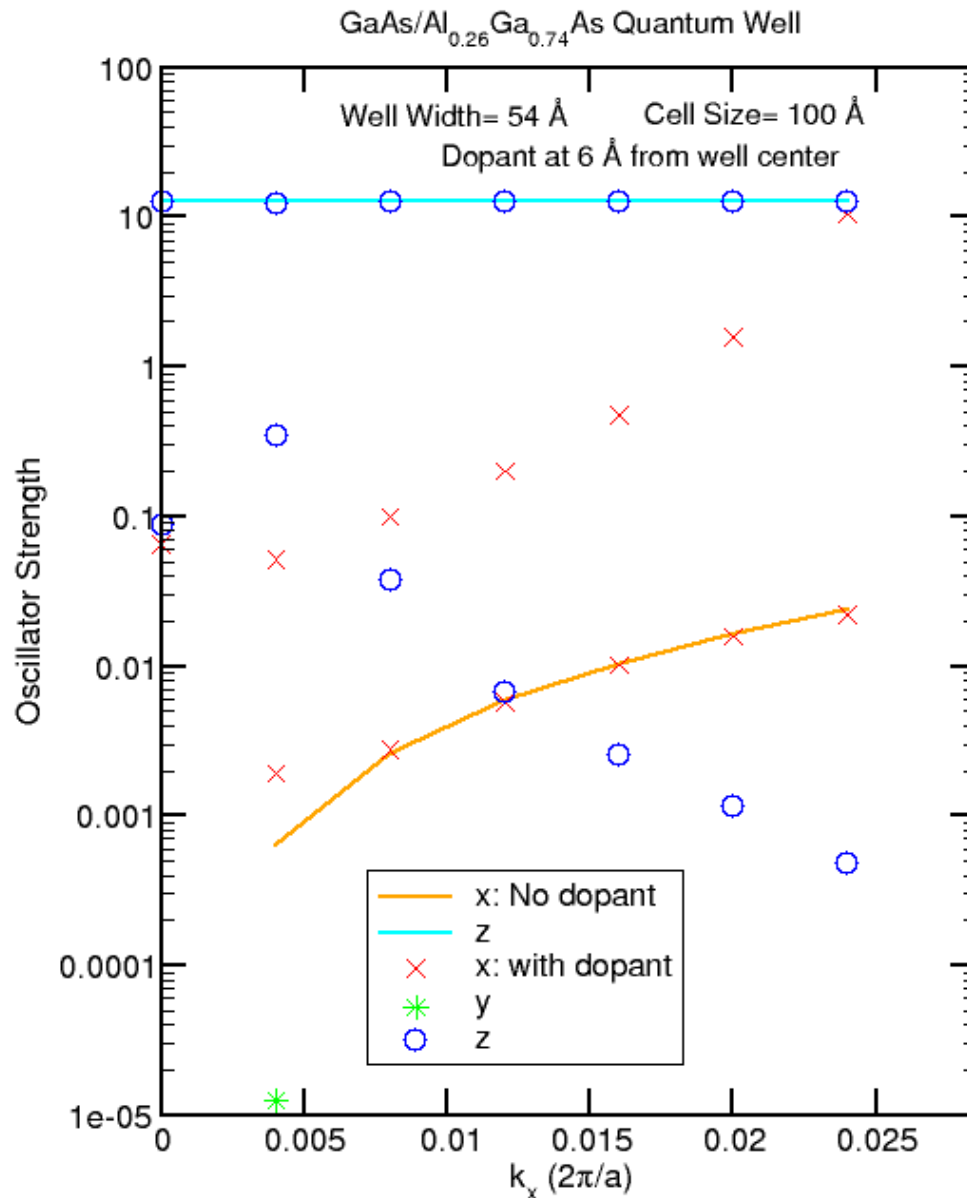
- With dopant, ground state energy vs. z-position (z=0 at edge, z=27 at well center)
- Green line is the ground state energy without dopants
- Single dopant simulation
- Different cell sizes used to simulate different doping concentration

Quantum Well Energy Levels with Dopant



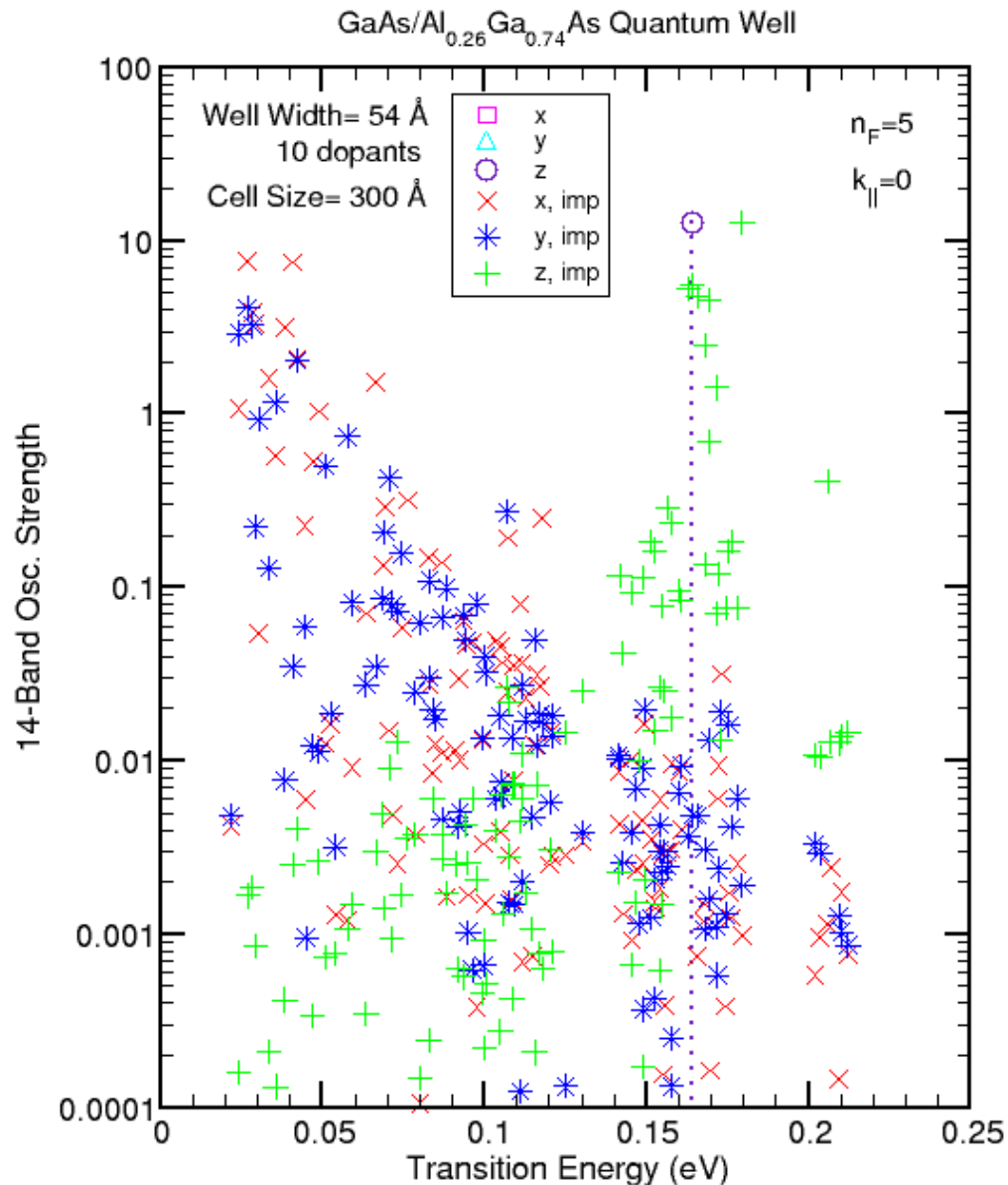
- A single dopant is placed in a supercell with 100 Å lateral dimensions
 - Dopant located at 6 Å from cell of the 54 Å wide GaAs well
- Dopant potential binding energy ~ few meV
- Supercell zone folding effects seen in energy levels

Dopant Effects on Oscillator Strengths



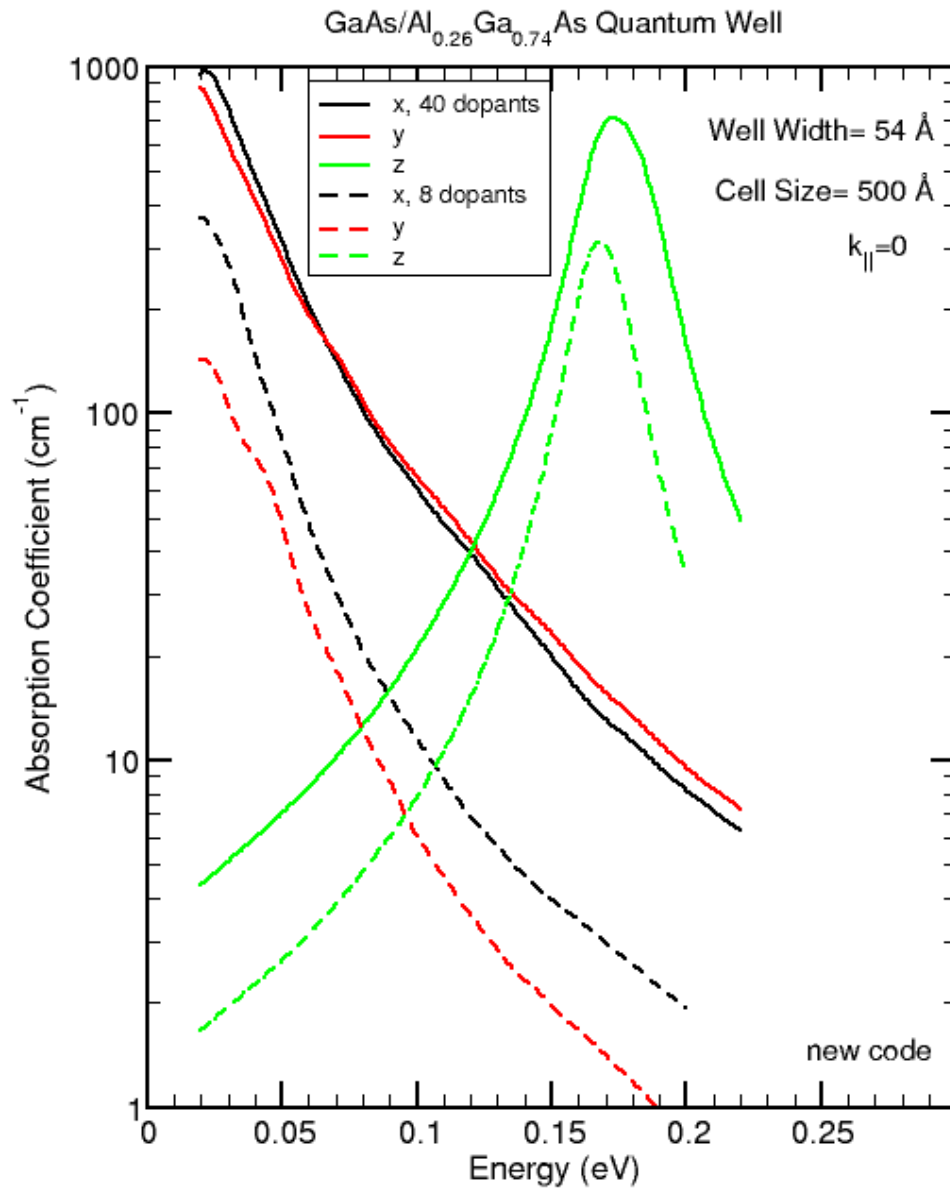
- Incorporation of dopant potential can increase the normal incidence oscillator strength
- More realistic simulations can be done using larger supercells with multiple randomly placed dopants

Dopant Effects on Oscillator Strengths



- Simulation geometry
 - Supercell with 300 Å lateral dimensions
 - 10 randomly placed dopants in QW region of supercell
- Oscillator strength computed with the lowest 5 energy levels filled
- Only z oscillator strength when there is no dopant potential
- Dopants induce normal incidence oscillator strengths.

Absorption Coefficient



- 40 impurities and 8 impurities
- Low energy: intrasubband;
- xy dominant

Quantum Dot

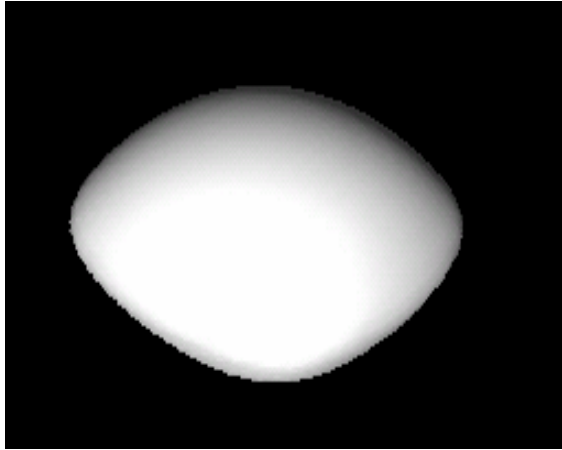
Simulation Geometry

InAs quantum dot embedded in GaAs

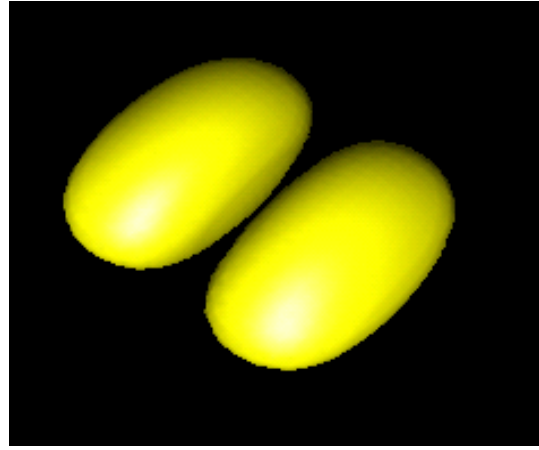
- Truncated pyramid (lens-shaped) QD
on wetting layer
 - Base width 265 Å
 - Dot height 25 Å
 - Wetting layer thickness 5 Å
 - Lens shaped dot
- Incorporate dopant potential
 - Single dopant
 - Vary lateral position
 - Vary vertical position

Charge densities of low-lying states in lens-shaped QD

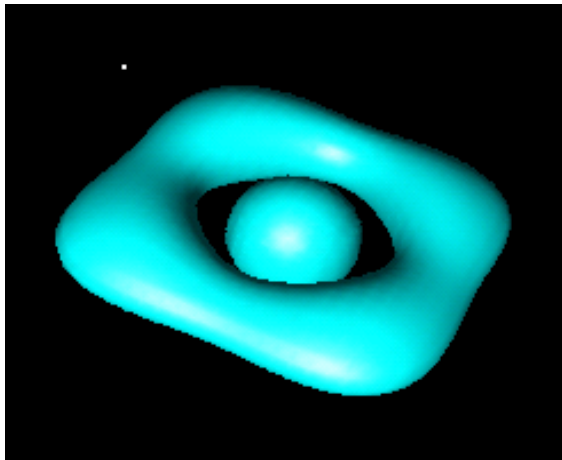
s-like



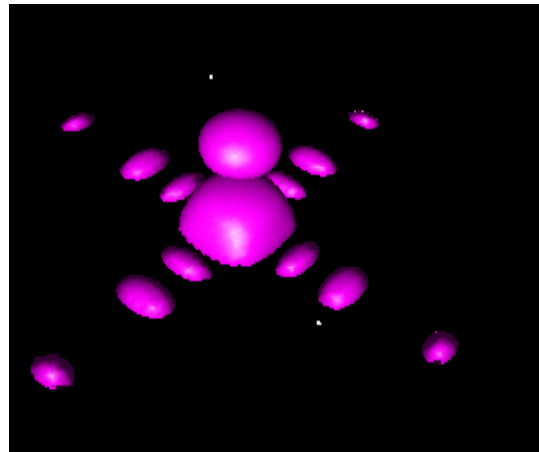
p_x/p_y like



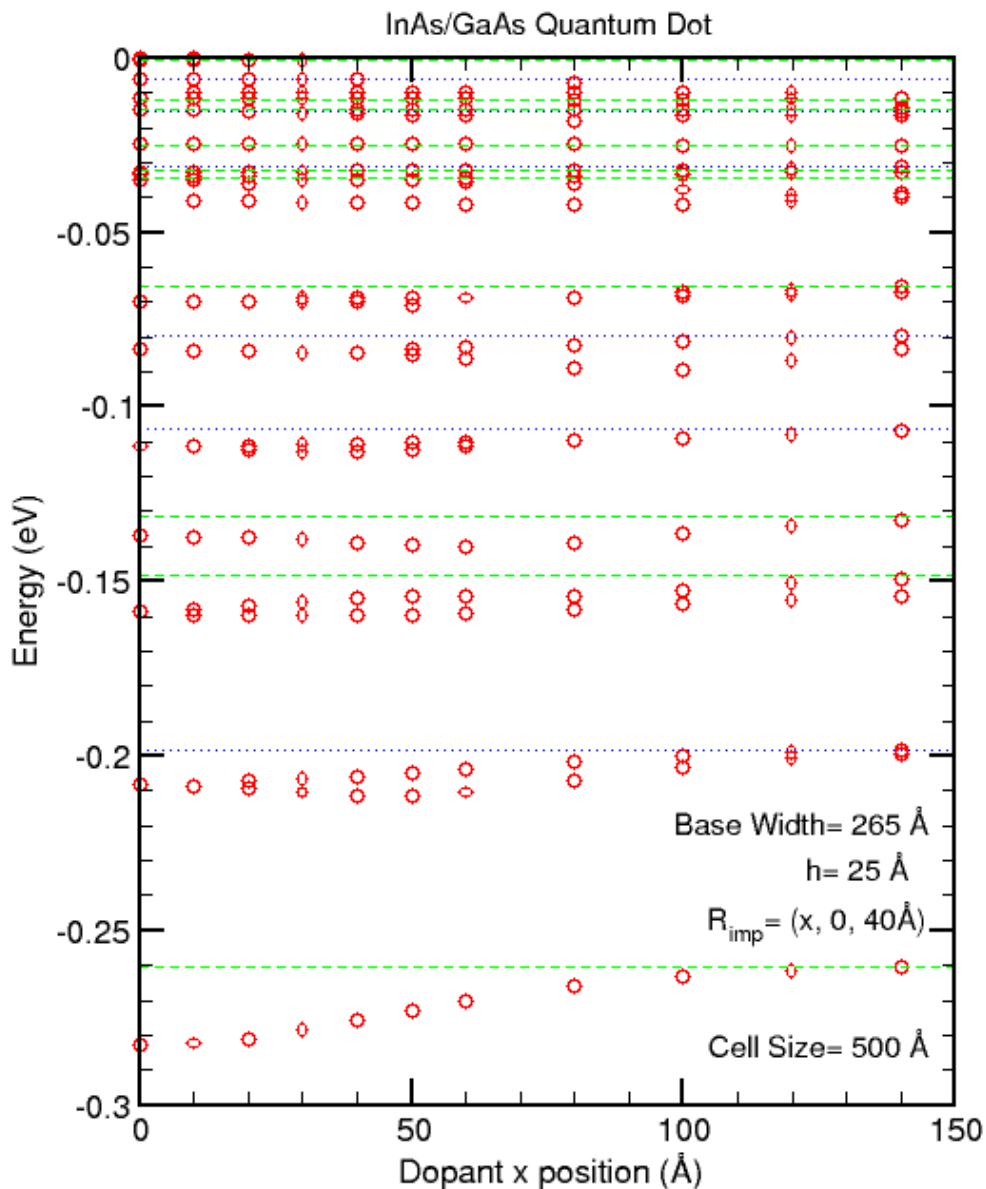
d-like



p_z like

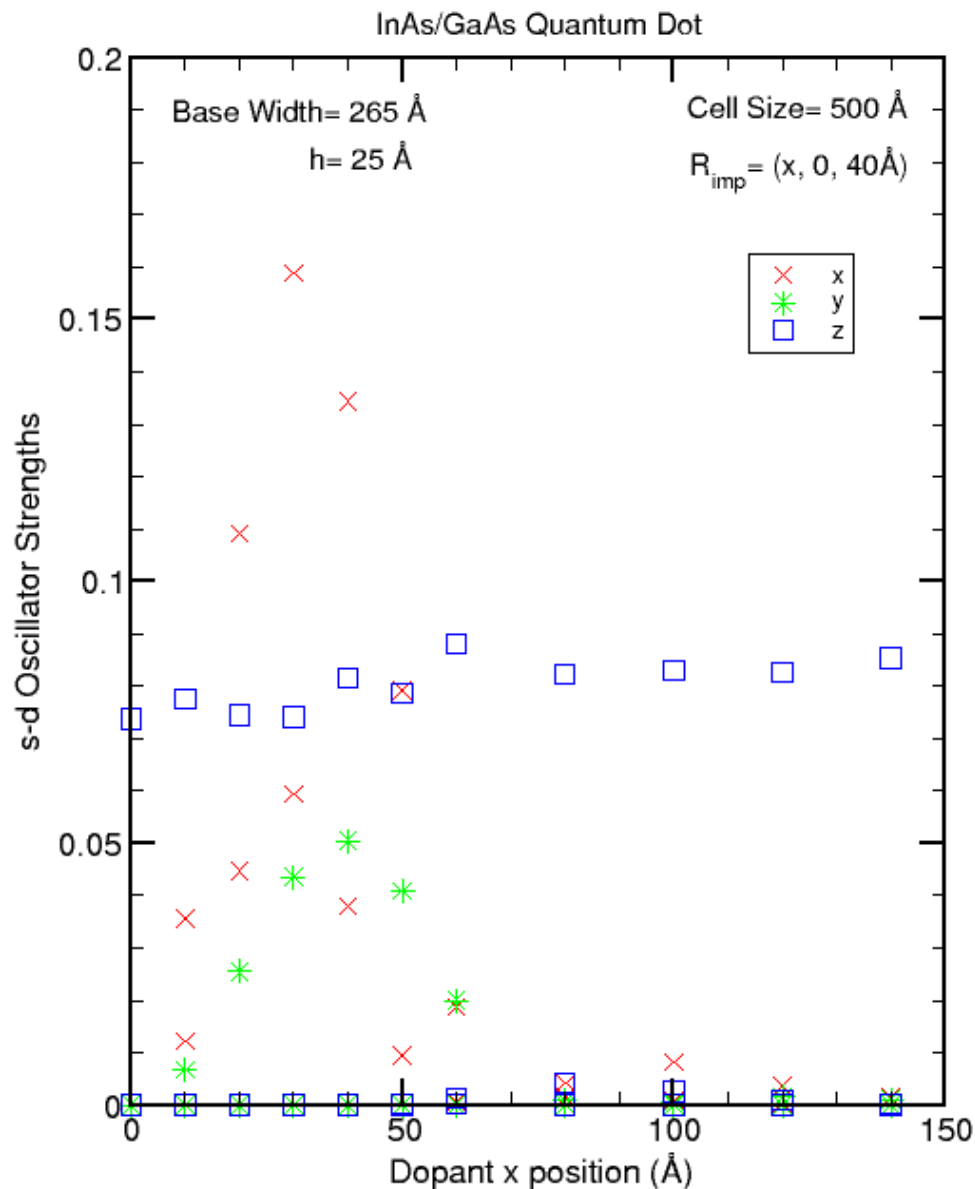


Quantum Dot with Dopant Impurity Energy Levels



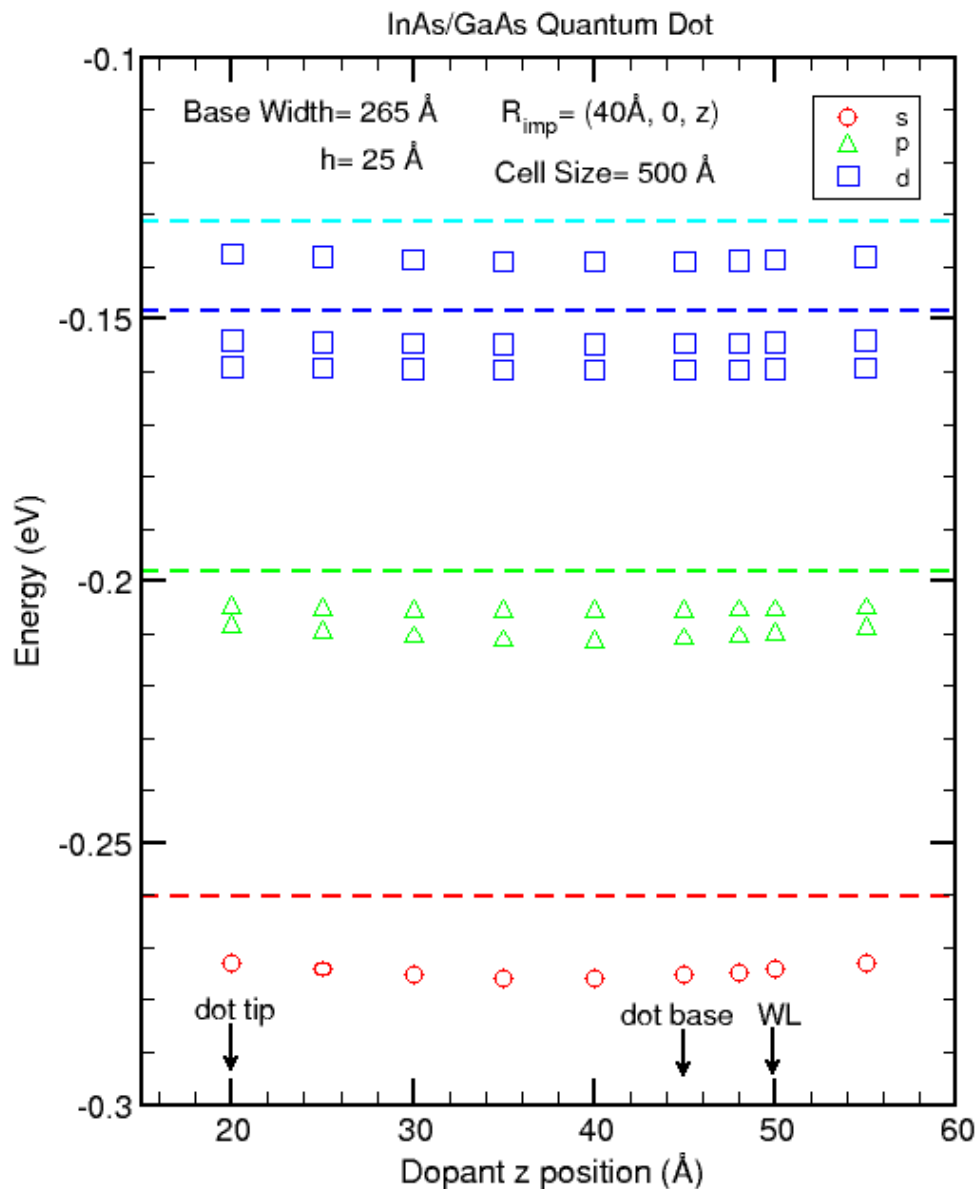
- Single dopant in a supercell
- Dopant position
 - Vary lateral (x) position
 - Vertical position fixed at 5 Å above top of wetting layer
- Energy level of QD with no dopant indicated by:
 - Green dashed line: even in x
 - Blue dotted line: odd in x
- Degeneracy removed by off center dopants

Effect of Dopant Potential on Oscillator Strengths



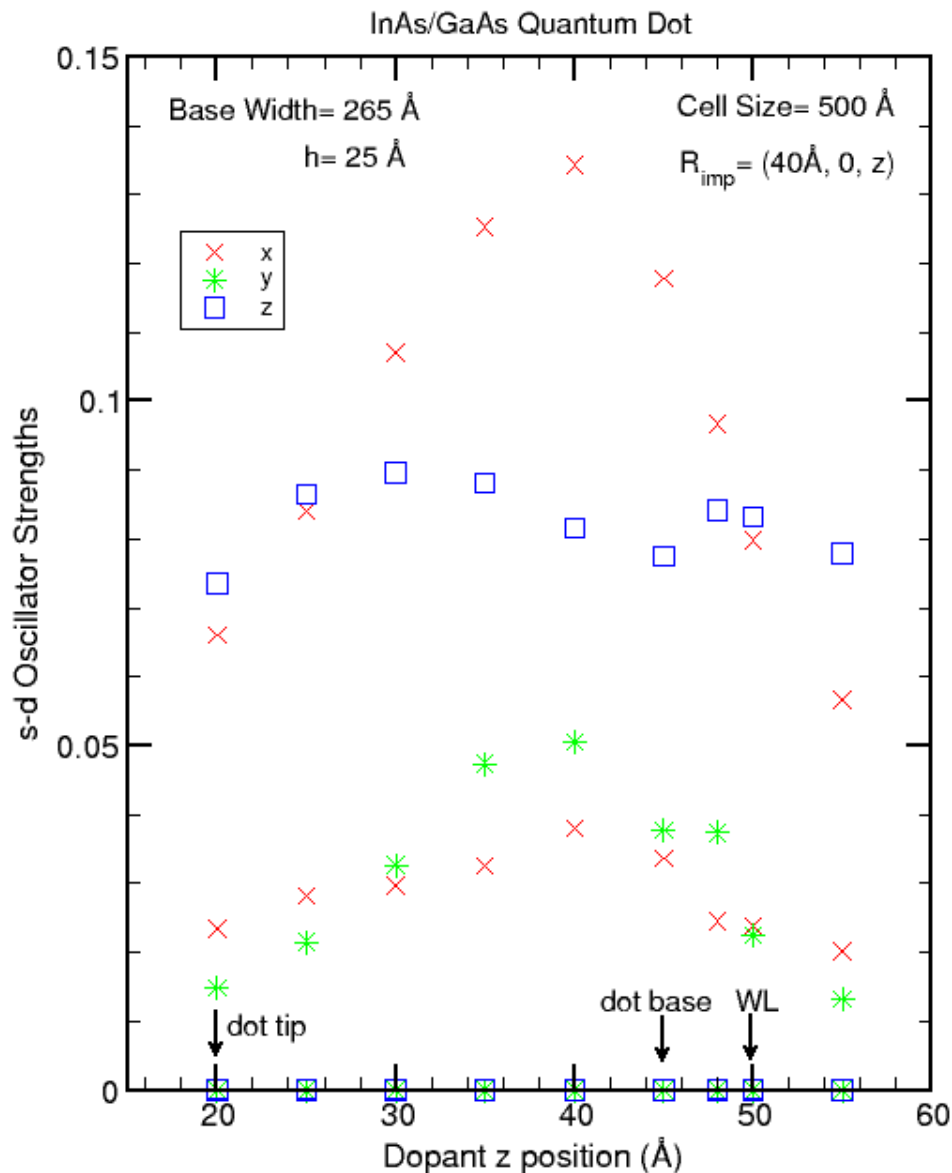
- Examine transitions from s-like ground state to 2nd set of excited states (d-manifold)
- No x oscillator strength without dopant potential
- With well-placed dopant, x oscillator strength can exceed z oscillator strength

Quantum Dot with Dopant Impurity Energy Levels



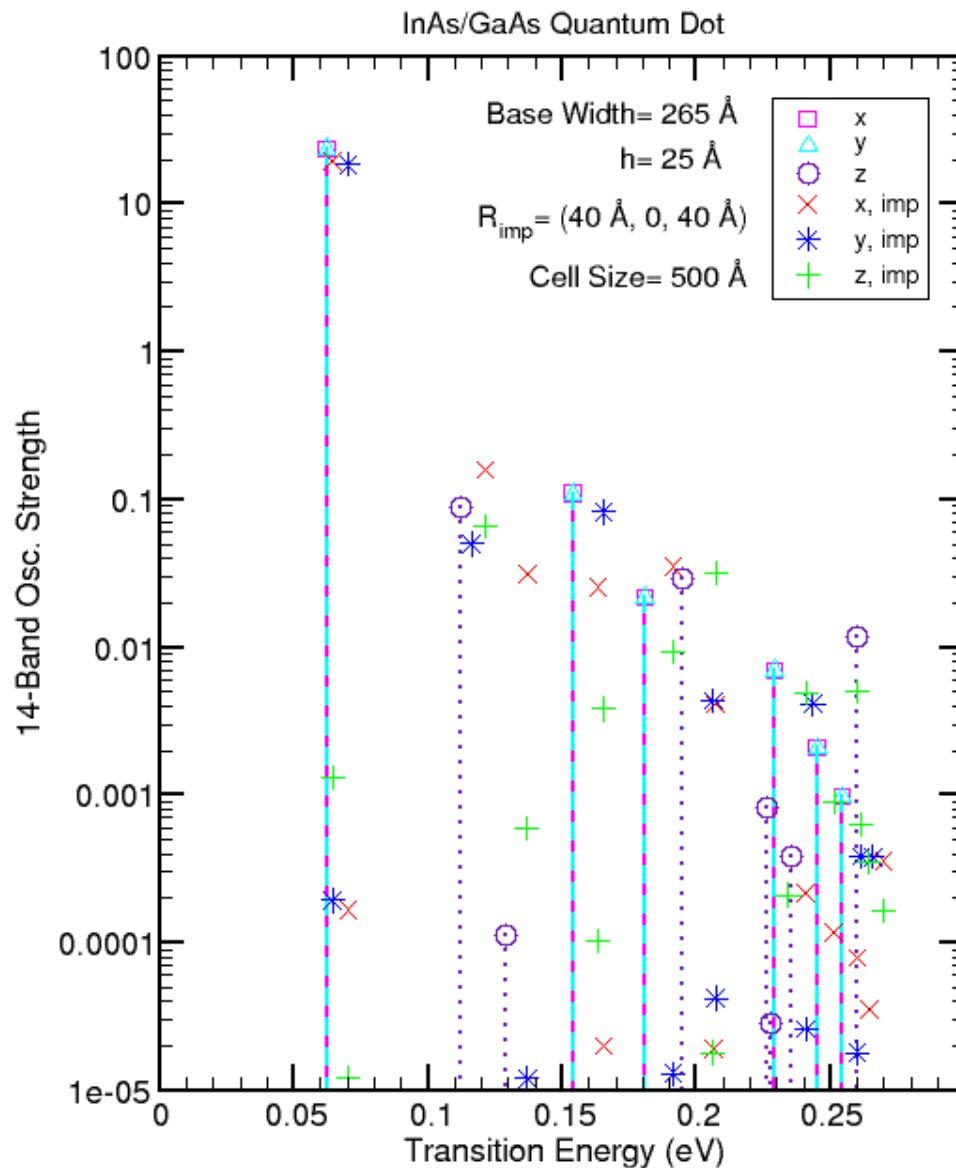
- Single dopant in a supercell
- Dopant position
 - Vary vertical (z) position
 - Lateral position fixed at 40 Å off center
- Energy level of QD with no dopant indicated by dashed lines
- Degeneracy removed by off center dopants

Effect of Dopant Potential on Oscillator Strengths



- Examine transitions from s-like ground state to 2nd set of excited states (d-manifold)
- Varying vertical position of dopant
- No x oscillator strength without dopant potential
- With well-placed dopant, x oscillator strength can exceed z oscillator strength

Effect of Dopant Potential on Oscillator Strengths



- Single dopant within the quantum dot
 - X: 40Å off center
 - Z: 5 Å above top of wetting layer
- No impurity oscillator strengths plotted as drop lines
 - X and y symmetric
- At transition energies above that of the fundamental (s-p) transition, dopant potential in general increases normal incidence oscillator strength at the expense of z oscillator strength

Summary

- Observed relatively strong normal incidence photoresponse in low-aspect ratio quantum dot devices
- Theoretical investigations indicate scattering due to dopant impurity potential could contribute to normal incidence response